Quaternary Geochronology 89 (2025) 101685

Contents lists available at ScienceDirect

Quaternary Geochronology

journal homepage: www.elsevier.com/locate/quageo

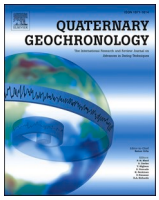

Reconstructing the Holocene volcanic past of El Hierro, Canary Islands

C. Prieto-Torrell [a,b], J.L. Fernandez-Turiel [c,*], A. Rodriguez-Gonzalez [d], M. Aulinas [a,b], E. Beamud [b,e], M.C. Cabrera [d], C. Criado [f], H. Guillou [g], P. Vidal-Matutano [f], F.J. Perez-Torrado [d]

[a] Departament de Mineralogia, Petrologia i Geologia Aplicada, Facultat de Ciències de la Terra, Universitat de Barcelona, Barcelona, Spain
[b] Geomodels Research Institute, Facultat de Ciències de la Terra, Universitat de Barcelona, Barcelona, Spain
[c] Geosciences Barcelona, GEO3BCN, CSIC, Barcelona, Spain
[d] Instituto de Estudios Ambientales y Recursos Naturales (i–UNAT), Universidad de Las Palmas de Gran Canaria (ULPGC), Las Palmas de Gran Canaria, Spain
[e] Paleomagnetic Laboratory CCiTUB-GEO3BCN, GEO3BCN, CSIC-UB, Barcelona, Spain
[f] ARQHISPA Research Group, Departamento de Geografía e Historia, Universidad de La Laguna, Spain
[g] Laboratoire des Sciences du Climat et de l'Environnement/IPSL, CEA-CNRS-UVSQ, Orme des Merisiers-RD 128, Gif-sur-Yvette, Cédex, F-91198, France

ARTICLE INFO

Keywords:
Radiocarbon dating
Paleomagnetic dating
$^{40}Ar/^{39}Ar$ dating
K-Ar dating
Anthracology
Volcanism
Holocene
El Hierro
Canary Islands

ABSTRACT

We present a geochronologic study with unprecedented detail from 42 Holocene subaerial volcanic edifices of El Hierro Island, Canary Islands. The study of new and published K-Ar, $^{40}Ar/^{39}Ar$, ^{14}C, and paleomagnetic ages, constrained by stratigraphic, geomorphic, and anthracological criteria, significantly improves the geochronologic framework of the Holocene volcanism at El Hierro. Our combined experiments show that radiocarbon and paleomagnetic dating were the best methods to determine this young volcanism's age. Indeed, small amounts of $^{40}Ar^*$ detected in most dated samples do not allow for calculating geologically significant ages. The preliminary anthracological study of charcoals is recommended before ^{14}C dating. Thirty-six eruptive events (86 % of the total) were retained for the geochronological model developed with ChronoModel combining radiocarbon and paleomagnetic and using the Bayesian inference. Seventeen eruptions were dated for the first time. The Holocene eruptive activity at El Hierro exhibits significant variability over time, with recurrence intervals ranging from 34 to 1078 years. The most recent subaerial eruptions were Lomo Negro, 1412 [1560, 1242] cal BP (MAP, mode of the posterior distribution, and 95 % highest posterior density (HPD) interval) and Montaña del Tesoro, 1059 [1206, 967] cal BP. In addition, historical records suggest possible submarine eruptions in 1721, 1777, and 1793, as well as the more recent and well-documented Tagoro volcano submarine eruption (2011–2012 CE). This recent low recurrence subaerial volcanic activity is unusual for an oceanic volcanic island in the juvenile shield growth stage. The volcanic edifices resulted from hybrid Strombolian monogenetic eruptions with alternating or simultaneous emission of pyroclastic tephra and lava flows. The absence of lava flows in the eruptions of the highest part of the island's summit is worth noting. This volcanic activity focused on the three rifts that configure the tetrahedral shape of the island, although the NW rift concentrated 50 % of the eruptions. These results contextualize the volcanic hazard of El Hierro in the face of eventual future eruptions.

1. Introduction

Effective volcanic risk mitigation is based on long-term basic research on volcanoes, with the interpretation of past active volcanism, especially establishing the location, type, style, and frequency of eruptions (Tilling, 1989). An area is generally considered to be volcanically active if it has undergone an eruption in the last 11700 years during the Holocene (Siebert et al., 2015). Reconstructing the Holocene eruptive history is essential to unravel volcanic/magmatic systems and mitigate future eruption damage (Malaguti et al., 2021; Nitta et al., 2020). The precise dating of recent volcanic eruptions is also important in geomorphologic, climatic, and archaeological studies, among others (Guilbaud et al., 2022; Holdaway et al., 2018; Mahgoub et al., 2017; Rufer et al., 2011).

The radiocarbon (^{14}C) dating of organic matter associated with a volcanic deposit formation or a paleosol below or above the studied unit may date it within the Holocene (e.g., Lockwood and Lipman, 1987). However, the difficulty of finding organic matter in volcanic deposits suitable for ^{14}C dating has led to alternative methods (Guilbaud et al., 2022). Other methods currently applied are K-Ar, $^{40}Ar/^{39}Ar$, and

* Corresponding author.
E-mail address: jlfernandez@geo3bcn.csic.es (J.L. Fernandez-Turiel).

https://doi.org/10.1016/j.quageo.2025.101685
Received 2 July 2024; Received in revised form 12 March 2025; Accepted 5 June 2025
Available online 13 June 2025

paleomagnetic dating, generally used by combining them in a complementary way. These methods can yield age indications directly from the eruptive materials. It remains a real challenge to date Holocene eruptions of a basaltic nature using K-Ar and $^{40}Ar/^{39}Ar$ methods. In fact, in these recent and low to moderately potassic rocks, the measurable radiogenic argon ($^{40}Ar^{*}$) content is low and close to the detection limits of mass spectrometers. The error margins at the ages determined in this way may be high. Nevertheless, without other dating sources, such as wood charcoal or zircon crystals that can be ^{14}C and U-Th dated, respectively, the K-Ar chronometer is often the only one that can be used. Moreover, combined with appropriate stratigraphic control, the paleomagnetic method could date the time of rock formation (Lerner et al., 2022; Risica et al., 2020, 2022; Vashakidze et al., 2019).

The island of El Hierro in the Canary Archipelago has not experienced subaerial eruptions since the European settlement in the fifteenth century (Romero Ruiz, 2016). Therefore, its volcanic hazard was usually perceived as low. This perception changed with the submarine eruption of the Tagoro volcano in 2011–2012 (Carracedo et al., 2012a, 2012b; Meletlidis Tsiogalos, 2017; Perez-Torrado et al., 2012). Nevertheless, the geologic record shows a wide variety of recent scoria cones and lava flows. The spectacular nature of these volcanic landforms led to the island's declaration as a UNESCO Global Geopark (UNESCO, 2023). This work aims to update our knowledge about the temporal evolution of the Holocene volcanism of the oceanic island of El Hierro to support more accurate prediction and characterization of its next likely activity. We conducted an extensive study on the recent volcanism of the island, using new and published K-Ar, $^{40}Ar/^{39}Ar$, ^{14}C, and paleomagnetic data coupled with stratigraphic and geomorphic criteria to ascertain the ages of 42 volcanic edifices and to reconstruct the Holocene eruptive history of El Hierro Island.

2. Study area

The study area comprises the land part of the El Hierro UNESCO Global Geopark (UNESCO, 2023), the island of El Hierro, Canary Islands, Spain. The Canary Islands archipelago is part of the Macaronesian region about 100 km off the northwest coast of Africa, between 29°25′ and 27°37′ N and 18°10′ and 13°20′ W (Fig. 1). The land area of the archipelago is about 7446 km^2, where 2,177,701 people lived in 2022 (ISTAC, 2023). The largest island is Tenerife, with 2034 km^2 (931,646 inhabitants in 2022), and the smallest is El Hierro, where 11,423 inhabitants lived in 2022 on an area of 269 km^2 (ISTAC, 2023).

The Canary Islands Archipelago comprises seven main islands and several islets and, with several seamounts, make up the Canary Islands Volcanic Province (CVP), a volcanic belt 800 km long and 400 km wide (e.g., Carracedo and Troll, 2016a, 2021). The CVP developed on the African plate, near the passive African continental margin, formed by a Jurassic oceanic lithosphere (old, cold, thick, and rigid crust). The age of the CVP volcanism decreases from NE to SW, from ca. 68 Ma at the Lars/Essaouira Seamount (Geldmacher et al., 2005) to ca. 1.12 Ma on the island of El Hierro (Guillou et al., 1996). This age progression is due to the relatively slow movement of the African plate (~2 cm/year; Silver

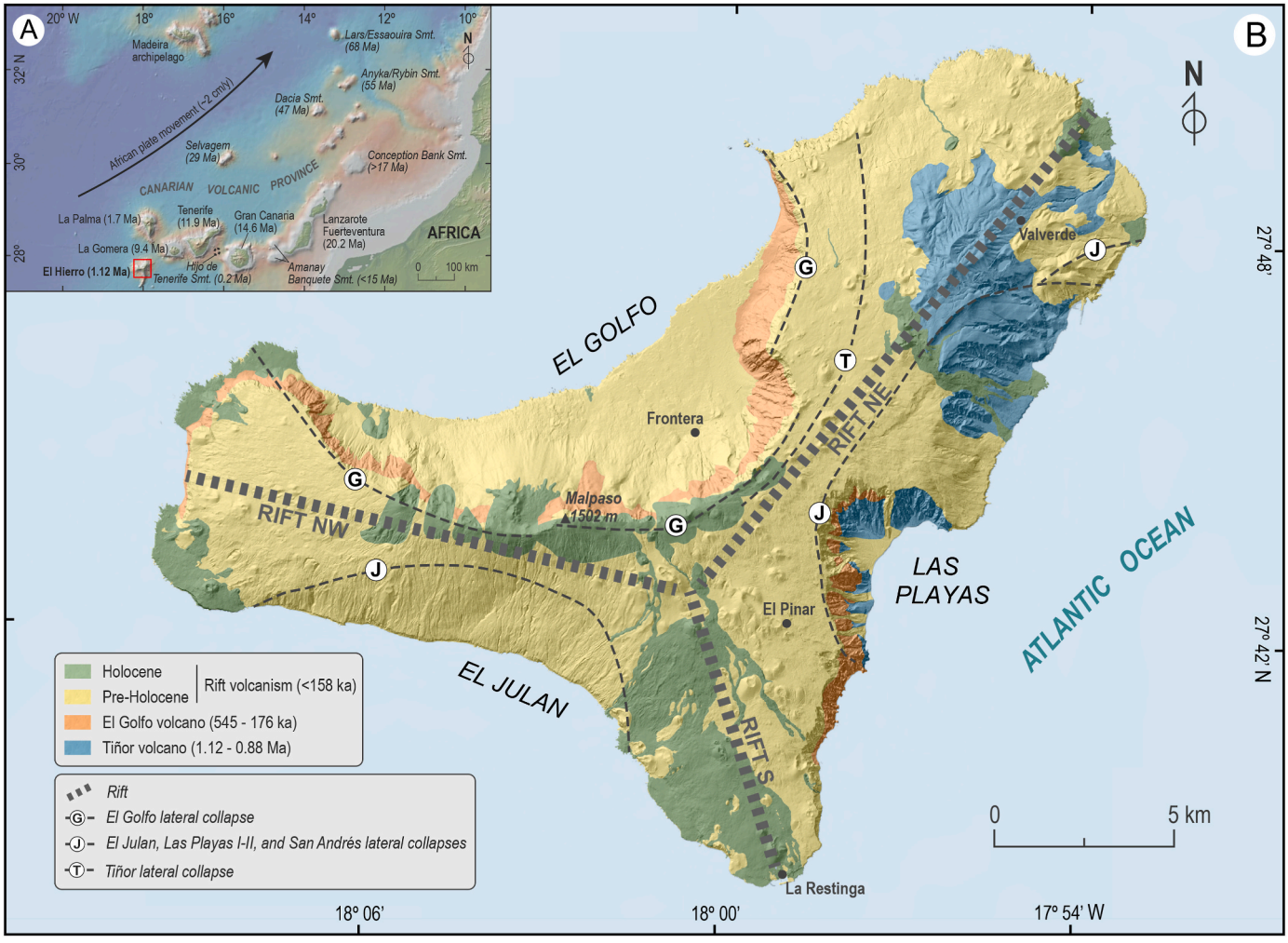

Fig. 1. A, Location of the El Hierro Island in the Canarian archipelago. B, Simplified geological map of the El Hierro Island (adapted from Carracedo et al., 2001; Balcells Herrera et al., 2010b, 2010a; Gómez Sainz de Aja et al., 2010b, 2010a).

et al., 1998) over a mantle plume (e.g., Hoernle and Schmincke, 1993; Carracedo, 1999; Geldmacher et al., 2005; Zaczek et al., 2015; Carracedo and Troll, 2016a, 2021).

The Canary Archipelago is volcanically active, and all the islands, except for La Gomera, show signs of Holocene volcanism. Lanzarote, Tenerife, La Palma, and El Hierro had historical eruptions. The historical period begins in the Canaries after 1402–1496 (Carracedo and Troll, 2016a; Guillén et al., 2023; Lobo Cabrera, 2019). The last subaerial eruption occurred at La Palma in 2021 (Tajogaite volcano; Carracedo et al., 2022, and references therein), while the last submarine eruption was in 2011 at the Tagoro volcano on El Hierro (Carracedo et al., 2012a, 2012b, 2015; Perez-Torrado et al., 2012).

El Hierro is the youngest and westernmost island in the Canarian Archipelago, and it is in the shield stage in the framework of the main stages of growth of oceanic volcanic islands, as defined in Hawaii (Clague and Sherrod, 2014). It rises from ~4000 m deep seafloor to 1502 m above sea level (a.s.l.) at the island's center (Pico de Malpaso). The most characteristic feature of El Hierro is its tetrahedral shape, with the three ridges (rift zones) at ~120° and separated by wide embayments associated with giant landslides (e.g., Guillou et al., 1996; Gee et al., 2001; Carracedo et al., 2001; Carracedo and Troll, 2016b) (Fig. 1). El Hierro exhibits a rugged relief, with steeply plunging cliffs, where the prominent volcanic landforms (cinder cones and lava flows) are well perceptible. Dissection by fluvial processes is poorly developed.

The island comprises three large overlapping volcanic edifices (Becerril et al., 2013, 2014, 2016a; Carracedo et al., 2001; Guillou et al., 1996; Meletlidis et al., 2023). The Tiñor volcano edifice (1.12–0.88 Ma) grew during the earliest period; later, the El Golfo volcano edifice (545–176 ka) was formed; and finally, the current rift volcanism (<158 ka) was consolidated, defining the structure, morphology, and distribution of the recent eruptions at El Hierro (e.g., Acosta et al., 2005; Carracedo, 1994, 1996, 1999; Gee et al., 2001b). The classification using the total alkali-silica (TAS) diagram (Le Bas et al., 1986), shows a largely basanitic composition for the Holocene volcanism (Prieto-Torrell et al., 2024; Prieto-Torrell et al., 2025). The rapid and unstable growth of the island promoted five giant gravitational landslides: Tiñor (<880 ka), Las Playas I (545–176 ka) and II (176–145 ka), El Julan (>158 ka), El Golfo (87-39 ka), and Punta del Norte (unknown age) (e.g., Urgeles et al., 1997; Carracedo, 1999; Carracedo et al., 2001; Masson et al., 2002; Longpré et al., 2011; Klimeš et al., 2023).

The first ages and geomagnetic polarities on the island of El Hierro were obtained by Abdel-Monem et al. (1972), and all corresponded to the Brunhes normal polarity chron. Fuster et al. (1993) also determined ages lower than 0.8 Ma. Guillou et al. (1996) and Széréméta et al. (1999) temporally framed the three large volcanic units of the island (Tiñor, El Golfo, and the volcanism of the rifts) and the giant landslides of Tiñor

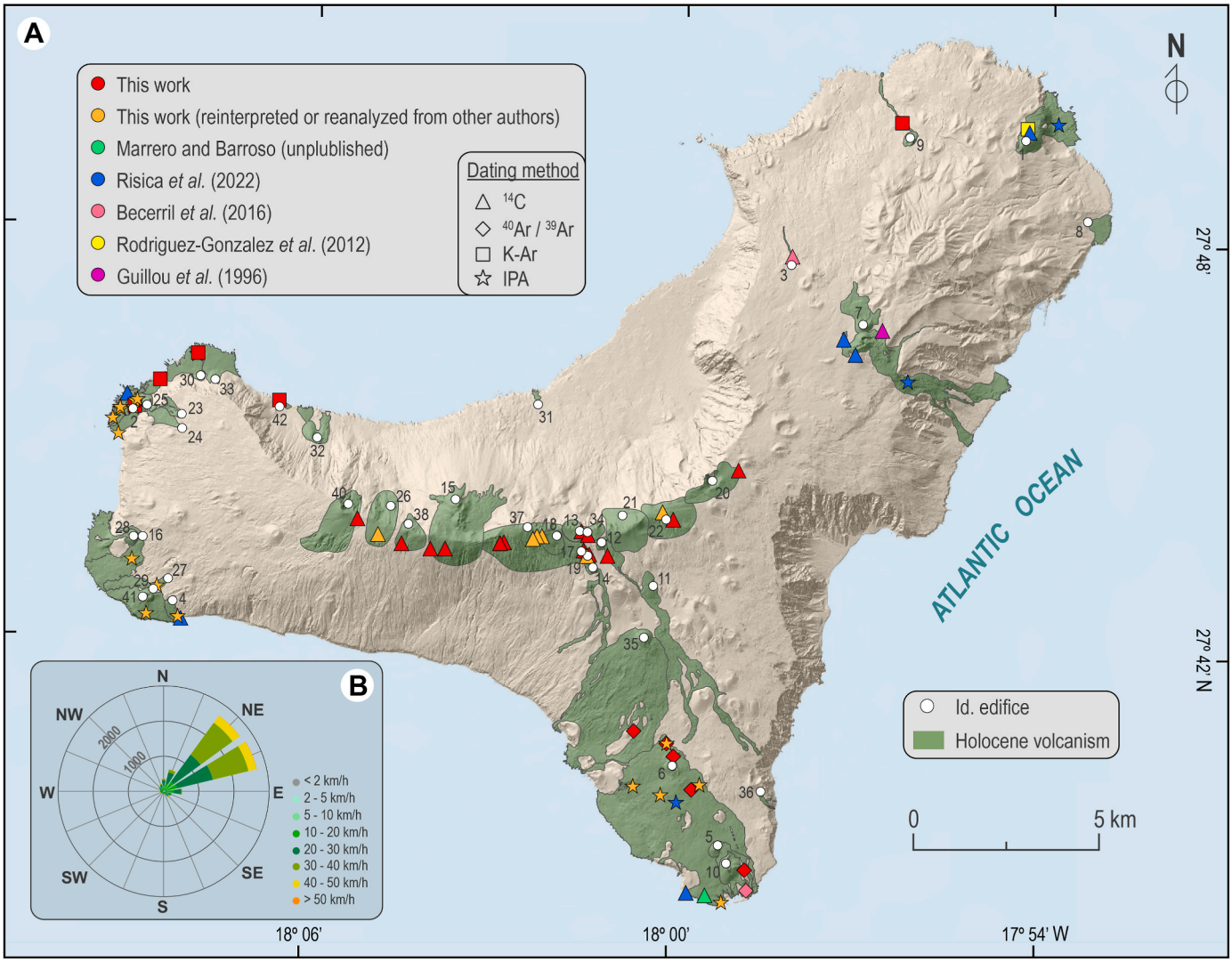

Fig. 2. A, Location of the 42 Holocene volcanic eruptions studied with the indication of the samples used to date them. IPA, inferred paleomagnetic age. Details of numbered edifices are in Table 1. B, The wind rose model shows how many hours per year the wind blows from the NE direction (Meteoblue, 2024).

and El Golfo. In addition, they obtained the oldest age (1.12 ± 0.02 Ma), demonstrating that El Hierro is the youngest island of the Canaries.

Despite the youth of El Hierro Island, no eruptions have been recorded onshore since 1402–1496, when the historical record began in the Canary Islands (Carracedo and Troll, 2016b; Guillén et al., 2023; Romero Ruiz, 2016). The only eruptions recorded on El Hierro were the possible submarine events of 1721, 1777, and 1793, as well as the Tagoro volcano in 2011 (Carracedo et al., 2012a, 2012b, 2015; Perez-Torrado et al., 2012; Romero Ruiz, 2016; Guillén et al., 2023). Concerning the subaerial Holocene volcanism (Fig. 2), the first ages were published by Pellicer (1977) (n = 2 ages, ^{14}C), which were followed by those of Hernández-Pacheco (1982) (n = 1, ^{14}C), Fuster et al. (1993) (n = 1, ^{14}C), Guillou et al. (1996) (n = 1, ^{14}C), Perez-Torrado et al. (2011) (n = 3, ^{14}C), Rodriguez-Gonzalez et al. (2012) (n = 1, K-Ar), Villasante-Marcos and Pavón-Carrasco (2014) (n = 1, paleomagnetism), and Becerril et al. (2016b) (n = 2, ^{14}C). Risica et al. (2022) documented the most recent and significant compilation, reporting eleven eruptions combining paleomagnetic and ^{14}C methods.

The climate of El Hierro is subtropical, moderated by the oceanic current from the Canary Islands and the prevailing NE trade winds (Fig. 2B). The orography and altitude significantly shape local weather conditions. The result is an altitudinal zonation BWh-BSh-BSk-Csb from the coast to the mountains according to the Köppen-Geiger climate classification (BWh, hot desert climate; BSh, hot steppe; BSk, cold steppe; Csb, dry and warm summers) (AEMET, 2012). The annual variation of the average air temperature ranges from 20 °C at sea level to 12 °C in the highlands (AEMET, 2012). Average annual rainfall varies between 100 and 800 mm/year due to orographic effects and exposure to NE trade winds. The rain shadow effect causes the northern flank of the island to receive the highest precipitation. Specific altitudinal vegetation belts are associated with different climatic zones (del Arco Aguilar et al., 2010). However, this theoretical climatophilous vegetation is modified by the humidity differences between the northern and southern flanks of the island. It has also been interrupted by the recent volcanic badlands that prevented its development. These features condition the possibility that an eruption generates charcoal that can be preserved and dated by the radiocarbon method.

3. Methods

3.1. Stratigraphic and geomorphic relationships

Detailed fieldwork on the recent volcanic edifices of El Hierro Island was carried out to establish their stratigraphic and geomorphic relationships (e.g., Prieto-Torrell et al., 2021). The edifices comprise lava flows and pyroclastic deposits related to scoria cones and tephra fall. Overlapping of lava flows from different eruptions or the surroundings of lava flows to previous volcanic cones and lava fields are examples of criteria that help us to order the volcanic edifices sequentially. For the isolated eruptions or not observed stratigraphic relationships (12 eruptions), the chronostratigraphic control is limited for radiometric ages or the formation of coastal lava deltas (Carracedo et al., 2001; Rodriguez-Gonzalez et al., 2022) (Fig. 3). On the other hand, a significant issue is the occurrence of two trachytic pumice deposits at the island's summit, which are excellent stratigraphic markers in the area. The upper corresponds to the Malpaso 1 volcanic edifice. The lower Malpaso 2 belongs to an unidentified previous edifice and occurs in small scattered outcrops (Fig. 4). Moreover, the relationships with the underlying or overlying paleosols were recognized to define the time framework more precisely (Fig. 5). These stratigraphic and geomorphic relationships have been documented in a dataset with 28 photographs illustrating the relationships among 27 of 42 Holocene eruptions investigated (Rodriguez-Gonzalez et al., 2024). Results are summarized in Table 1. This information was the basis for sampling and interpreting the materials used for dating.

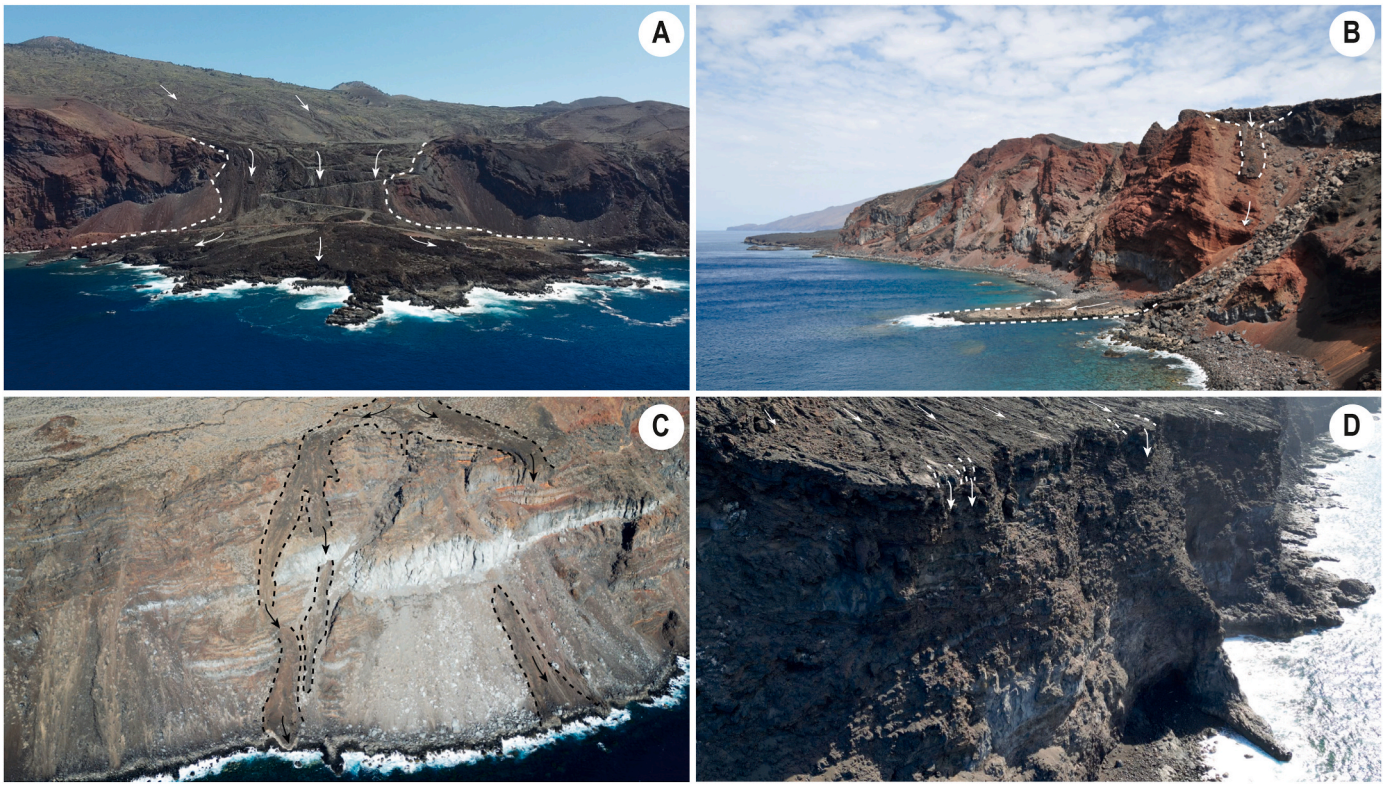

Fig. 3. Lava deltas and lava flow remnants on coastal cliffs are geomorphic evidence of eruptions younger than 7000 years. A, Lava delta of the Montaña de la Empalizada volcano (Id. 35). B, Lava delta of the El Lajial edifice (Id. 6, Luna event). C, Remnants of lava flows on the coastal cliff of the Calderetones edifice (Id. 36). D, Lava flow remnants on the coastal cliff of the Montaña de Orchilla edifice (Id. 41).

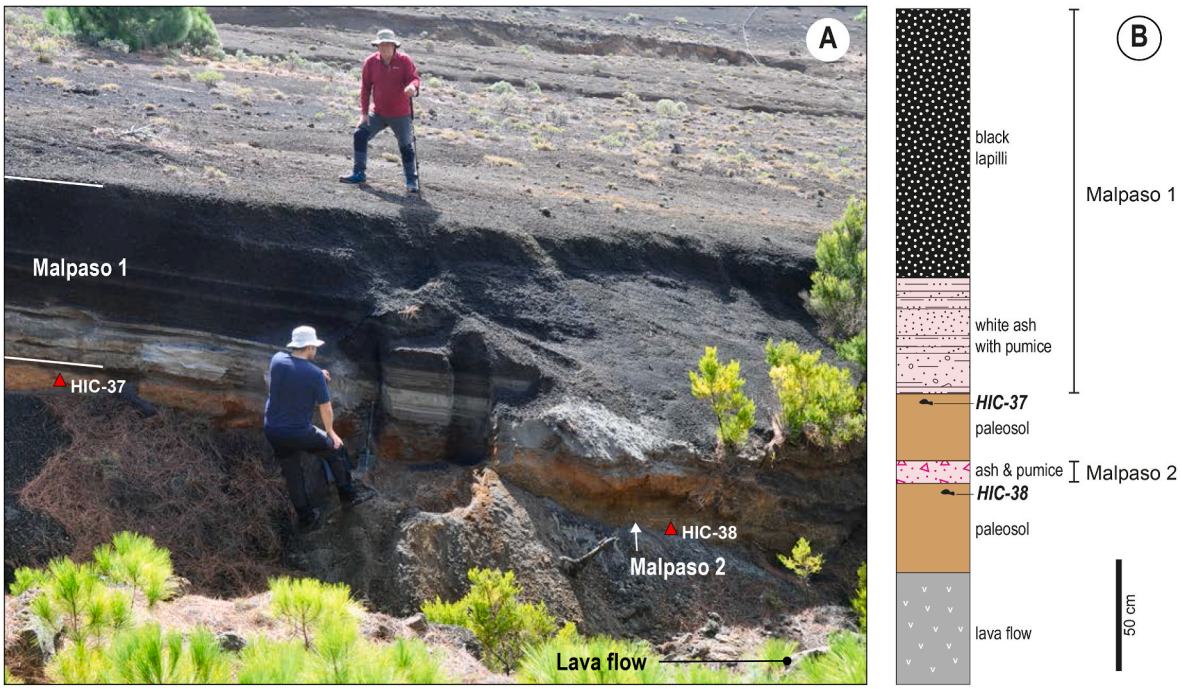

Fig. 4. Stratigraphic section where the charcoal samples HIC-37 and HIC-38 were collected (see data in Table 1). A, General view of the outcrop. B, Simplified stratigraphic column.

3.2. Unspiked K-Ar and $^{40}Ar/^{39}Ar$ dating methods

The proven effectiveness of the combined unspiked K-Ar and $^{40}Ar/^{39}Ar$ dating methods in the ^{14}C age range for dating recent lavas from the Canary archipelago (Guillou et al., 2011) led us to select these two methods as potential for dating Holocene volcanic activity at El Hierro. Concerning the unspiked K-Ar method, our choice seems appropriate as it has been successfully used to date Holocene volcanism at El Hierro (Guillou et al., 1996) and La Palma (Guillou et al., 1998). In the case of La Palma, we even showed agreement between K-Ar and ^{14}C ages for a lava flow as young as 3 ka (K-Ar age = 4 ± 2 ka and ^{14}C age = 3.2 ± 0.1 ka). Because we have presented both methods in several of our papers dealing with the Canary Archipelago volcanism, sample processing and the two dating methods are described in the electronic supplement S01. Seven samples were dated by the unspiked K-Ar method (Suppl. S02), and we used the $^{40}Ar/^{39}Ar$ technique to date six other lava flows (Suppl. S03-S04-S05).

3.3. Radiocarbon dating methods

We collected charcoal samples for radiocarbon dating from 15 sites (Figs. 2 and 4-5; Suppl. S06-S07). We sampled 14 stratigraphic sections because samples HIC-37 and HIC-38 correspond to the same stratigraphic profile of Malpaso 1 and 2 (Fig. 4). Except for the HIC-17 (Morro de las Sanjoras) and HIC-39 (Montaña del Cepón) samples, the rest were collected in the paleosol underlying the volcanic material, always looking for the location closest to the contact between both units. The age obtained represents the maximum age for the eruption, but it is close enough to the actual age so that it is the one to work with for practical purposes. It was verified that the charcoal samples were fragments without lateral continuity, which could indicate their nature as roots charred by recent wildfires. The HIC-17 sample was collected within a trunk mold in a pyroclastic deposit, and the HIC-39 under a lava flow. It is interpreted that both samples originated by combustion due to the eruptive process; therefore, the age obtained corresponds to the age of the eruption.

A discrepancy in age for the Malpaso 1 trachytic pumice deposit led to speculation that the charcoal samples dated at the island summit by Perez-Torrado et al. (2011) derive from plant roots of the current soil burned by forest fires (Pedrazzi et al., 2014). To settle this controversy, we conducted an anthracologic study of the samples HIC-18, HIC-21, HIC-22, and HIC-23. Each charcoal fragment was fractured manually to provide transverse, tangential, and radial sections for taxonomic identification using a Brunel SP-400 bright/dark field incident light microscope with 50–600x magnification at the University of La Laguna, Spain. Botanical identification was performed using specialized plant anatomy literature (Montagnoli et al., 2021; Peterson et al., 1999; Schweingruber, 1990) and a modern charred, woody taxa reference collection. All the available charcoal samples were analyzed. Photography and detailed observations of the anatomical and taphonomic features were carried out using a Zeiss EVO MA 15 scanning electron microscope (SEM) at the General Research Support Service (SEGAI), University of La Laguna, Spain.

Radiocarbon dating of charcoal samples was carried out by Accelerator Mass Spectrometry (AMS) at the laboratories of Beta Analytic Inc. (Miami) and 14CHRONO Centre of Queen's University (Belfast). To complete this dataset, we added additional radiocarbon data of charcoals published by Pellicer (1977) (n = 2), Guillou et al. (1996) (n = 1), Perez-Torrado et al. (2011) (n = 3), Becerril et al. (2016a,b) (n = 1), Risica et al. (2022) (n = 8), as well as of a goat horn by Marrero and Barroso (unpublished) (n = 1) and marine mollusk shells (n = 2) (Risica et al., 2022) (Suppl. S07). The conventional ages were rounded as recommended by the community (Stuiver and Polach, 1977).

The calibration of new and published radiocarbon data was performed by ChronoModel v. 3.0 (Lanos and Dufresne, 2023, 2024) using the IntCal20 (intcal20.14c) atmospheric curve (Reimer et al., 2020). For marine shells, we used the global marine calibration curve Marine20 (marine20.14c) (Heaton et al., 2020) and the local marine reservoir correction for the Canary Islands, ΔR of −201.9 ± 32.4 ^{14}C years, obtained by Santana et al. (2024).

3.4. Paleomagnetic dating methods

Paleomagnetic dating is based on acquiring a stable thermoremanent

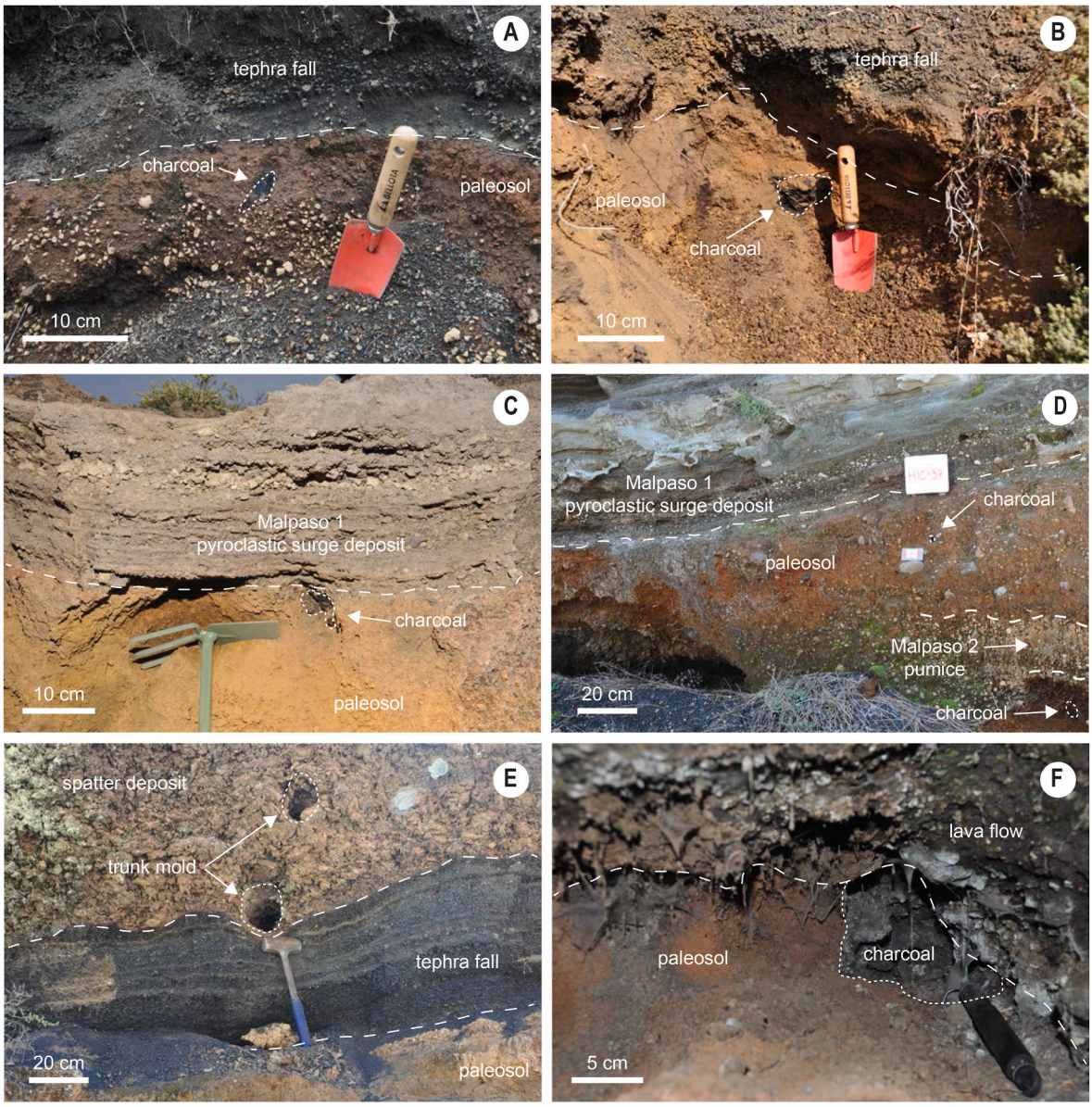

Fig. 5. Charcoal samples for radiocarbon dating in paleosols underlying the tephra fall deposits. A, Mt. de los Humilladeros (Id. 40, HIC-05). B, Pico de los Marrubios (Id. 22, HIC-30). C, Malpaso 1 (Id. 37, HIC-22). D, Malpaso 1 and Malpaso 2 charcoals (Ids. 37 and 39, HIC-37-38) provide the maximum-limiting ages for the overlying pyroclastic deposits. E, HIC-17 sample at the Morro de las Sanjoras (Id. 19) eruption from within a trunk mold embedded in pyroclasts. F, HIC-39 beneath a lava flow of the Montaña del Cepón (Id. 12) eruption. We interpret in E and F that the charcoal originated from combustion during the eruptions; therefore, fixing the age of the eruption.

magnetization parallel and proportional to the geomagnetic field present during the lava flow cooling since magmatic temperatures are higher than Curie temperatures of the magnetic minerals it contains. The eruption age of lava can be estimated by comparing the paleodirection (and paleointensity, if available) inferred from the thermoremanent magnetization with the paleosecular variation (PSV) curve of the study region (e.g., Pressling et al., 2009; Alva-Valdivia et al., 2019; Risica et al., 2020, 2022).

At El Hierro, Villasante-Marcos and Pavón-Carrasco (2014) focused their study on the Lomo Negro eruption lava flows (6 sampling sites), and Risica et al. (2022) extensively studied the Holocene volcanism of the island (37 sampling sites on 9 lava flows). We revised these paleomagnetic data according to the new ages, stratigraphic relationships, and geomorphic criteria discussed in this work. This revision led to the reinterpretation of the assignment of some sampling sites to certain eruptions and, accordingly, new paleomagnetic ages were attained for the reinterpreted sites (Suppl. S08).

The ages were obtained following the methodology described by Lanos (2004) and implemented online in ArchaeoPyDating, the new release of *archaeo_dating* software (Pavón-Carrasco et al., 2011, 2014). The tool has been adapted to Python and is now presented as an online application (Serrano et al., 2024). It provides the global model SHA. DIF.14k (12000 BC - 1900 AD) (Pavón-Carrasco et al., 2014) to estimate the corresponding age intervals. This software package uses a Bayesian statistical approach to assign age ranges within which an undated discrete paleomagnetic record with normally distributed uncertainty correlates with a dated master record at a predefined confidence level. Probability density functions (PDFs) were computed separately for declination and inclination and combined into a single PDF. Results were calculated to a 95 % level of confidence. The resulting PDFs and inferred ages discussed below are shown in the Suppl. Table S08 and Fig. S09.

Table 1
Summary of Holocene subaerial volcanic edifices of El Hierro Island.

Id. edifice	Volcanic edifice	Rift	Location in the island			Vent coordinates		Characteristics*	Stratigraphic relationships	Geomorphic constraint
			summit	extreme	other	Latitude (°N)	Longitude (°E)			
1	Montaña del Tesoro	NE		extreme		27.825144	−17.907134	SE [CC + T + L]	Isolated	Formed lava delta
2	Lomo Negro	NW		extreme		27.754970	−18.148693	SE [SV + L]	Over 23, 24, 25	
3	Montaña del Cascajo	NE			other	27.793706	−17.970237	SE [CC + L]	Isolated	
4	Montañita Negra	NW		extreme		27.708667	−18.136623	SE [CC + L]	Over 41	Formed lava delta
5	Montaña de Prim	S		extreme		27.652503	−17.986553	SE [CC + L]	Over 6, 10	Formed lava delta
6	El Lajial	S		extreme		27.671570	−17.999453	CE [CC + SV + L]	Over 10, 35, under 5	Formed lava delta
7	Montaña Chamuscada	NE			other	27.779641	−17.950330	CE [CC + L]	Isolated	Formed lava delta
8	La Caleta	NE		extreme		27.805840	−17.889726	SE [CC + L]	Isolated	Formed lava delta
9	Montaña de Aguarijo	NE		extreme		27.825223	−17.938708	SE [CC + L]	Isolated	Formed lava delta
10	La Restinga	S		extreme		27.648157	−17.984195	CE [CC + SV + L]	Under 5, 6	Formed lava delta
11	Cueva del Mocán	S			other	27.715053	−18.005792	SE [CC + L]	Over 12, 35	Lava flow remnants on the coastal cliff
12	Montaña del Cepón	S	summit			27.725316	−18.020132	SE [SV + L]	Over 21, under 11	
13	Monumento al Campesino Herreño	S	summit			27.727944	−18.026183	SE [CC + T]	Over 34, 37	
14	Montañita del Guanche de Abajo	S	summit			27.719168	−18.022364	SE [CC + L]	Over 19, 35	
15	Tanganasoga	NW	summit			27.734926	−18.060240	CE [CC + T + L]	Over 37, 39	
16	El Meridiano	NW		extreme		27.724079	−18.145174	SE [SV + L]	Over 28, 29	Formed lava delta
17	El Brezal	S	summit			27.723018	−18.025618	SE [SV + L]	Over 37	
18	Pino Verde	S	summit			27.726644	−18.032402	SE [CC + T]	Over 37 (inferred)	
19	Morro de las Sanjoras	S	summit			27.721982	−18.023856	SE [SV + L]	Over 37, 39, under 14	
20	Hoya de Fireba	NE	summit			27.740919	−17.990396	SE [CC + T]	Over 22 (inferred)	
21	Pico Tenerife	NE	summit			27.730447	−18.009918	SE [CC + T]	Over 22 (inferred), under 12	
22	Pico de los Marrubios	NE	summit			27.731243	−18.002692	SE [CC + T]	Under 20 (inferred), 21 (inferred)	
23	Montaña de Marcos	NW		extreme		27.753941	−18.135393	SE [CC + L]	Over 24, 25, 30, under 2	Formed lava delta
24	Montaña de los Guirres	NW		extreme		27.750520	−18.135195	SE [CC + SV + L]	Over 25, under 2, 23	Formed lava delta
25	Hoya del Verodal	NW		extreme		27.755970	−18.144897	SE [CC + L]	Under 2, 23, 24	Formed lava delta
26	Monte Grande	NW	summit			27.732928	−18.077815	SE [CC + T]	Not observed	
27	El Estacadero	NW		extreme		27.713994	−18.138008	SE [SV + L]	Over 29	
28	Montaña de las Calcosas	NW		extreme		27.724050	−18.147649	SE [CC + L]	Under 16	Formed lava delta
29	La Hoya del Faro	NW		extreme		27.711747	−18.141477	SE [SV + L]	Over 41, under 16, 27	
30	Roque de Basco	NW		extreme		27.763406	−18.130496	SE [CC + L]	Over 33, under 23	Formed lava delta
31	Charco Azul	NW			other	27.758381	−18.038373	SE [SV + L]	Isolated	Formed lava delta
32	Sabinosa	NW			other	27.749083	−18.098310	SE [CC + L]	Isolated	Formed lava delta
33	Arenas Blancas	NW		extreme		27.762583	−18.126492	SE [CC + L]	Under 30	Formed lava delta
34	Cruz de los Reyes	S	summit			27.727731	−18.024056	SE [CC + T]	Under 13	
35	Montaña de la Empalizada	S			other	27.702470	−18.007987	SE [CC + L]	Under 6, 11, 14	Formed lava delta
36	Calderetones	S		extreme		27.665811	−17.975233	CE [SV + L]	Isolated	Lava flow remnants on the coastal cliff
37	Malpaso 1	NW	summit			27.728580	−18.040423	SE [CC + T + S]	Over 39, under 13, 15, 17, 18 (inferred), 19	
38	Picos de la Peña del Agua	NW	summit			27.728674	−18.072863	SE [CC + T]	Not observed	
39	Malpaso 2	?	summit			unknown		SE [S]	Under 15, 19, 37	
40	Montaña de los Humilladeros	NW	summit			27.733156	−18.089383	SE [CC + T]	Not observed	
41	Montaña de Orchilla	NW		extreme		27.709405	−18.144747	SE [CC + L]	Under 4, 29	Lava flow remnants on the coastal cliff
42	Lomo Cabras	NW			other	27.756289	−18.108775	SE [SV + L]	Isolated	Lava flow remnants on the coastal cliff

* SE, single edifice; CE, complex edifice; CC, cinder cone (fall and surge deposits); SV, spatter vent (fissure or cone); T, tephra fall deposit; S, surge deposit; L, lava flow.

3.5. Geochronological framework modeling using Bayesian inference

To reconstruct a robust chronology for the Holocene volcanism of El Hierro, we employed a Bayesian target event date model (Lanos and Philippe, 2017, 2018) implemented in ChronoModel v. 3.2.7 (Lanos and Dufresne, 2023, 2024). This approach integrates ^{14}C and paleomagnetic geochronological data alongside stratigraphic and geomorphic constraints.

The model leverages a hierarchical Bayesian statistical framework and Markov chain Monte Carlo (MCMC) numerical techniques to estimate event dates and their uncertainties. Numerical (absolute) dates from bracketing units and relative stratigraphic and geomorphic

Table 2
Ages of Holocene subaerial volcanic edifices of El Hierro Island. MAP, mode of the posterior distribution. HPD, highest posterior density region.

Id. edifice	Volcanic edifice	MAP [prob 95 % HPD range]	MAP [prob 95 % HPD range] (tentative temporal position)	Unmodeled age (tentative temporal position)
		(cal BP)	(cal BP)	(cal BP)
1	Montaña del Tesoro	1059 [1206, 967]		
2	Lomo Negro	1412 [1560, 1242]		
3	Montaña del Cascajo	2322 [2540, 1988]		
4	Montañita Negra	2033 [2599, 1780]		
5	Montaña de Prim		1216 [2537, 248]	
6	El Lajial	2548 [2581, 2503]		
7	Montaña Chamuscada	3601 [3723, 3400]		
8	La Caleta			<7000 - >454
9	Montaña de Aguarijo			<7000 - >454
10	La Restinga		4837 [8591, 2399]	
11	Cueva del Mocán		2057 [3282, 239]	
12	Montaña del Cepón	3348 [3500, 3135]		
13	Monumento al Campesino Herreño	3669 [4035, 3347]		
14	Montañita del Guanche de Abajo		2505 [4233, 197]	
15	Tanganasoga	4869 [5078, 4342]		
16	El Meridiano	4138 [4619, 3676]		
17	El Brezal	4189 [4488, 3930]		
18	Pino Verde	4395 [4906, 3909]		
19	Morro de las Sanjoras	4547 [4756, 3922]		
20	Hoya de Fireba	4582 [4974, 4251]		
21	Pico Tenerife	4361 [5029, 3328]		
22	Pico de los Marrubios	5010 [5307, 4844]		
23	Montaña de Marcos		3502 [5231, 2190]	
24	Montaña de los Guirres	4872 [5379, 3845]		
25	Hoya del Verodal	5299 [5399, 5189]		
26	Monte Grande	5794 [6080, 5575]		
27	El Estacadero	5661 [6583, 4785]		
28	Montaña de las Calcosas		5294 [8587, 3895]	
29	La Hoya del Faro		7390 [11004, 5503]	
30	Roque de Basco	5854 [6551, 5139]		
31	Charco Azul			<7000 - >454
32	Sabinosa			<7000 - >454
33	Arenas Blancas		6457 [8458, 5441]	
34	Cruz de los Reyes	6508 [6763, 6269]		
35	Montaña de la Empalizada	5430 [8354, 3015]		
36	Calderetones			<7000 - >454
37	Malpaso 1	6744 [6838, 6585]		
38	Picos de la Peña del Agua	6872 [7121, 6620]		
39	Malpaso 2	7657 [7825, 6946]		
40	Montaña de los Humilladeros	7075 [7390, 6791]		
41	Montaña de Orchilla	8929 [9827, 7984]		
42	Lomo Cabras			<17000 - >454

positions serve as prior information.

Individual eruptions were defined as discrete events characterized by associated ^{14}C and/or paleomagnetic data. Three MCMC chains were run, comprising 1000 burn-in, 1000 adaptation (200 max batches), and 100,000 acquisition iterations with a thinning rate of 10. The model generates posterior distributions for event dates, summarized by the mode of the posterior distribution (MAP) and the 95 % highest posterior density (HPD) interval. Event dates are reported as calibrated ranges of years before the present (considered 1950 CE). For example, the geochronological model for the Mt. del Tesoro eruption/event provided a date of 1059 [1206, 967] cal BP (MAP [95 % HPD range]) (Table 2).

4. Results

4.1. Studied eruptions

We studied 42 subaerial volcanic edifices on the island of El Hierro based on the hypothesis that they were generated by eruptions during the Holocene (Fig. 2). Although there are probably some other edifices from this epoch, the group studied comprises most of the Holocene subaerial volcanism on El Hierro. The coordinates and toponyms of the main vents, used to name the edifices, are presented in Table 1.

The style of these monogenetic eruptions at El Hierro Island is Strombolian. The edifices were created by hybrid eruptions with alternating, or, more often, contemporaneous emission, of pyroclastic tephra, forming cones and fall deposits, and lava flows, whether they are a'a' or pahoehoe or with both types in the same event. Some edifices are complex and were generated in several episodes that have been differentiated when possible. Such is the case of La Restinga (Id. 10) and El Lajial (Id. 6), where we have distinguished six and fifteen construction episodes, respectively. A typical current example is the 2021 Tajogaite volcano eruption on La Palma Island (Bonadonna et al., 2022; Carracedo et al., 2022). It is worth noting the absence of lava flows in the eruptions recorded at the highest part of the summit of El Hierro Island (e.g., Montaña de los Humilladeros, Id. 40).

4.2. Stratigraphy and geomorphology

The overlapping of some edifices allowed us to recognize stratigraphic relationships with relative ease (e.g., Lomo Negro, Id. 2, over Montaña de Marcos, Id. 23; Montaña de los Guirres, Id. 24; and Hoya del Verodal, Id. 25) and establish the temporal succession order among many eruptions (Table 1) (Rodriguez-Gonzalez et al., 2024). Unfortunately, the edifices are sometimes isolated (e.g., Montaña del Tesoro, Id.

1; Calderetones, Id. 36), or these relationships are not well exposed (e.g., Monte Grande, Id. 26; Picos de la Peña del Agua, Id. 38). Despite these limitations, the stratigraphic relations are an independent relative age control to assess dating results. On the other hand, the top of the island exposes two trachytic pumice deposits that are reliable stratigraphic markers (Fig. 4). The upper one is Malpaso 1 (Id. 37), the lower one is Malpaso 2 (Id. 39).

Lava deltas on contemporary coastal platforms constrain an eruption age at El Hierro (Rodriguez-Gonzalez et al., 2022). This criterion allows us to estimate that an eruption occurred during the last 7000 years. On the other hand, the remnants of a lava flow on a coastal cliff are not as conclusive as lava deltas in absolute age. Still, they indicate the youth of the eruption (Fig. 3). Eighteen lava flows formed deltas around the island, and at least four lava flow remnants are preserved on the coastal cliffs (Table 1).

4.3. Unspiked K-Ar dating

The K-Ar results are summarized in Suppl. S02. Of the seven samples, three yielded Holocene ages ranging from 8 to 10 ka with uncertainties from 2 to 6 ka: Montaña del Tesoro (Id. 1), HIR-005, 9 ± 6 ka; Montaña de Marcos (Id. 23), HIR-013, 8 ± 2 ka; and Arenas Blancas (Id. 33), HIR-009, 8 ± 2 ka. The other four samples gave pre-Holocene ages: basement of Montaña del Tesoro, HIR-007, 21 ± 2 ka; Lomo Negro (Id. 2), HIR-018, 111 ± 2 ka; Montaña de Aguarijo (Id. 9), HIR-004, 18 ± 4 ka; and Lomo Cabras (Id. 42), HIR-020, 17 ± 1 ka. Among the last group, the age of a cliff-forming lava flow in the basement of the volcanic edifice of Montaña del Tesoro (21 ± 2 ka) is consistent with the age of this edifice (9 ± 6 ka). However, the other ages are older than expected. The case of the Lomo Negro edifice is noteworthy, with an unlikely age of 111 ± 2 ka when its lava flows are stratigraphically above the lava flows of the eruption Id. numbers 23-24-25, the two latter dated as Holocene. Excess argon is a possible cause for overestimated K-Ar ages.

4.4. $^{40}Ar/^{39}Ar$ dating

The $^{40}Ar/^{39}Ar$ results are summarized in Suppl. S03-S04-S05. The spread of experimental points along the inverse isochrones is very narrow (i.e., from 0 to 1.9 %). This feature, combined with very low 40Ar* contents close to the detection limits of the mass spectrometer, results in highly inaccurate isochron ages. However, these samples appear to be free of excess argon. Indeed, the $^{40}Ar/^{36}Ar$ interception values are similar to those of the atmospheric one. In the following, we use plateau ages, which are a little more precise.

Only one of the six dated samples gave a useful age. Indeed, sample HIR-156, a lava flow below the pyroclastic sequence of Morro de las Sanjoras and Malpaso 1 and 2 (Fig. 6), gave an age of 18.9 ± 6.2 ka, consistent with the radiocarbon ages of samples HIC-17, HIC-21, HIC-22, HIC-37, and HIC-38. Regarding the other samples, their ages are too imprecise to be useful (i.e., the error being higher than the age value).

4.5. Radiocarbon dating

The new results of 15 charcoal samples and the 18 published ages (15 from charcoal, one from goat's horn, and two from mollusk shells) compose a dataset of 33 radiocarbon ages (Suppl. S07). The map of Fig. 2 reflects that charcoal samples are more abundant in central/higher altitudes. The difficulty of finding datable charcoal is a limitation in extensive areas of the island due to the vegetation distribution associated with climate stratification and the occurrence of vast lava flow fields, locally known as '*malpaís*', that hinder vegetation growth.

It should be noted that volcanic environments may be subject to dilution of atmospheric CO_2 by magmatic CO_2, which does not contain ^{14}C (Hatté and Jull, 2025). This phenomenon has been the subject of different studies. Examples include the anomalously old age (^{14}C) of aquatic moss, which may be an effect of geothermal water in Iceland (Sveinbjörnsdóttir et al., 1992), the ^{14}C depletion of different C3 plants (leaves) growing inside and outside degassed volcanic zones in the Azores (Pasquier-Cardin et al., 1999), and the increase in the apparent age of fossil apatites in calcined bones by dead carbon near Pompeii in Italy (Zazzo and Lepetz, 2017). Furthermore, prevailing winds may also influence the resulting CO_2 mix. Plant macrofossils could inherit this dilution, leading to apparent radiocarbon ages older than their actual ages. The impact of these features could affect some observed ages, which are discussed below.

The anthracological studies of the organic samples guaranteed reliable radiocarbon dating results. Previous botanical determination and taphonomic analysis are necessary to select the most suitable taxon and the sample with the least biodegradation to date (Pardo-Gordó et al., 2022). The anthracological study of samples HIC-18, HIC-21, HIC-22, and HIC-23 allowed us to select specific charcoal fragments for radiocarbon dating. A total of 68 charcoal fragments were studied. Microscopic viewing of the xylem structure shows all charcoal derived from trunk/branch fragments and could be identified to species or family-level classification. Identified taxa consist of *Pinus canariensis* (Canary Island pine), *Erica arborea* (heather), and Fabaceae (the legume family) (Fig. 7). These taxa are consistent with the characteristic vegetation of the central area of the island (La Cumbre area) where pine forests and *fayal-brezal* forests develop above 600 m a.s.l. (Kämmer, 1976; Pérez de Paz et al., 1981; Rivas Martínez, 1987). Several Fabaceae species, such as *Adenocarpus foliolosus* or *Spartocytisus filipes*, among others, develop in the pine forest and the limits of the laurel forest.

The sample HIC-18 yielded eleven fragments of *Erica arborea* charcoal (Fig. 7A and B); HIC-21, 22 of Fabaceae charcoal (Fig. 7D-E-F); HIC-22, one of *Erica arborea* charcoal (Fig. 7C) and six of *Pinus canariensis* (Fig. 7G-H-I); and HIC-23, one fragment of *Erica arborea* charcoal and six of *Pinus canariensis*. Three samples were dated using *Erica arborea* charcoal (HIC-18, HIC-22, and HIC-23) and one with Fabaceae charcoal (HIC-21) (Suppl. S07).

Several edifices have two or more radiocarbon ages: Malpaso 2 (Id. 39, n = 2), Malpaso 1 (Id. 37, n = 6), Pico de los Marrubios (Id. 22, n = 2), Morro de las Sanjoras (Id. 19, n = 2), Tanganasoga (Id. 15, n = 3), Montaña Chamuscada (Id. 7, n = 3), and El Lajial (Id. 6, n = 2). The three first cases are on the summit ridge of the island (La Cumbre area). When we consider this area as a whole, it is observed that many of the charcoal samples (n = 24) have been sampled in paleosols (n = 16, 67 %). A set of 23 ages (70 % of the total) was included in the geochronological model for Bayesian inference.

4.6. Paleomagnetic dating

We carefully revised the existing dataset of paleomagnetic ages on lava flows of Holocene eruptions of El Hierro provided by Risica et al. (2022), samples labeled "HIE", and Villasante-Marcos and Pavón-Carrasco (2014), samples "LN" (Suppl. S08). This review led to the reinterpretation of the assignment of some volcanic edifices where Risica et al. (2022) collected the samples. This screening provided paleomagnetic information (declination, inclination, and α_{95}) on 17 eruptive events to estimate the corresponding age intervals based on the global SHA.DIF.14k model (Pavón-Carrasco et al., 2014) with the ArchaeoPyDating tool. Stratigraphy, geomorphology, and the lack of subaerial eruptions historically recorded after 1496 were used as constraints to select the 17 age intervals used for Bayesian inference to build the geochronological model (Suppl. S08-S09-S10).

4.7. Geochronological framework modeling using Bayesian inference

The K-Ar and $^{40}Ar/^{39}Ar$ dates provided ages with uncertainties too great to be meaningful from a geological point of view, so they were discarded for the geochronological model. Despite this, most of them confirmed the youthfulness of the dated lavas, demonstrating their value

Fig. 6. Stratigraphic section at the site where lava flow sample HIR-156 and charcoal sample HIC-21 were collected. The ages of both samples are consistent with each other, and with those for Malpaso 1 and Morro de las Sanjoras edifices.

in preliminary screenings of geochronological studies of Holocene eruptions at El Hierro (Guillou et al., 1996).

A set of 36 eruptive events (86 % of the total) were retained for the geochronological model developed with ChronoModel combining radiocarbon and paleomagnetic and using the Bayesian inference. Seventeen eruptions were dated for the first time.

Fifteen events were dated using radiocarbon data, four using a combination of radiocarbon and paleomagnetic data, and seven using only paleomagnetic data. From 16 volcanic edifices to which it has not been possible to obtain an absolute age, ten were included in the model based on the constraints defined by the stratigraphic record, the geomorphic criteria of formation or not of lava deltas, and the lack of subaerial eruptions during the last 500 years. The remaining six edifices, which are isolated (e.g., Sabinosa, Id. 32, or La Caleta, Id. 8), have not been included in the model. Their stratigraphic position was established by subjective comparison with the dated edifices based on the degree of erosion and weathering (observing, e.g., the smoothing of surface texture, development of weathering rinds, degree of vesicle preservation, or development of jointing patterns and carved channels), or the development of vegetation.

The ChronoModel input data and the summary of Bayesian age sequence modeling results are presented in Suppl. S10. Fig. 8 shows the posterior distribution graphs for probability densities of the eruption ages predicted by the Bayesian age sequence model. The calibration results of radiocarbon ages not included in the model are shown in Suppl. Table S11.

5. Discussion

By applying Bayesian inference through ChronoModel software, we statistically integrated geochronological data to construct a novel and refined model of Holocene subaerial eruptive activity on El Hierro. The outcomes of this geochronological modeling are summarized in Table 2. These results represent a substantial step forward in our knowledge of recent volcanism in El Hierro. Nevertheless, significant challenges persist due to the limited availability of geochronological data for certain eruptive events, constrained only by stratigraphic and geomorphological evidence. Within these limitations, we propose a tentative reconstruction of the temporal succession of all studied eruptive events (Table 2).

The temporal distribution of eruptive events in El Hierro differs from the discrete eruptive periods observed in Gran Canaria, presenting a nearly continuous sequence without significant hiatuses as occurs on the island of Tenerife (Carracedo et al., 2007; Rodriguez-Gonzalez et al., 2009).

Recent advancements in understanding El Hierro's volcanism have led to an increased estimate of eruptive recurrence, aligning with the island's juvenile shield stage of this oceanic volcanic island. Becerril et al. (2014) documented 25 eruptions over the past 158 ka, while Becerril et al. (2016b) identified at least 31 onshore eruptions in the last 33 ka. Furthermore, Abis et al. (2023) recognized at least 40 eruptions in the southern rift within the past 40 ka.

Eruptive recurrence intervals, derived from 20 consecutive MAP ages (Table 2, Fig. 8), exhibit significant variability. The median interval was 288 years, the mean was 346 years, with a standard deviation of 300 years, and a range of 34–1078 years. Only six eruptions have been recorded in the past 2000 years: two onshore (Montaña del Tesoro, Id. 1, and Lomo Negro, Id. 2) and four submarine (in 1721, 1777, 1793, and the Tagoro volcano in 2011–2012 CE) (Guillén et al., 2023).

The three rifts of El Hierro were active during the Holocene. However, the NW rift concentrated 50 % of the eruptions (n = 21) (e.g., Lomo Negro, Id. 2). The southern rift had 13 eruptions (31 %) (e.g., El Lajial, Id. 6), and the NE rift eight eruptions (19 %) (e.g., Montaña del Tesoro, Id. 1). It is noteworthy that 19 eruptions (45 %) occurred in the coastal ends of the rifts (e.g., Hoya del Verodal, Id. 25), 16 eruptions (38 %) in the summit of the island (e.g., Malpaso 1, Id. 37), and seven eruptions (17 %) (e.g., Montaña Chamuscada, Id. 7) in other locations (Table 1).

5.1. Rift NW

Despite extensive information on El Hierro's Holocene volcanism after 7000 BP, uncertainty remains for the early Holocene, when we

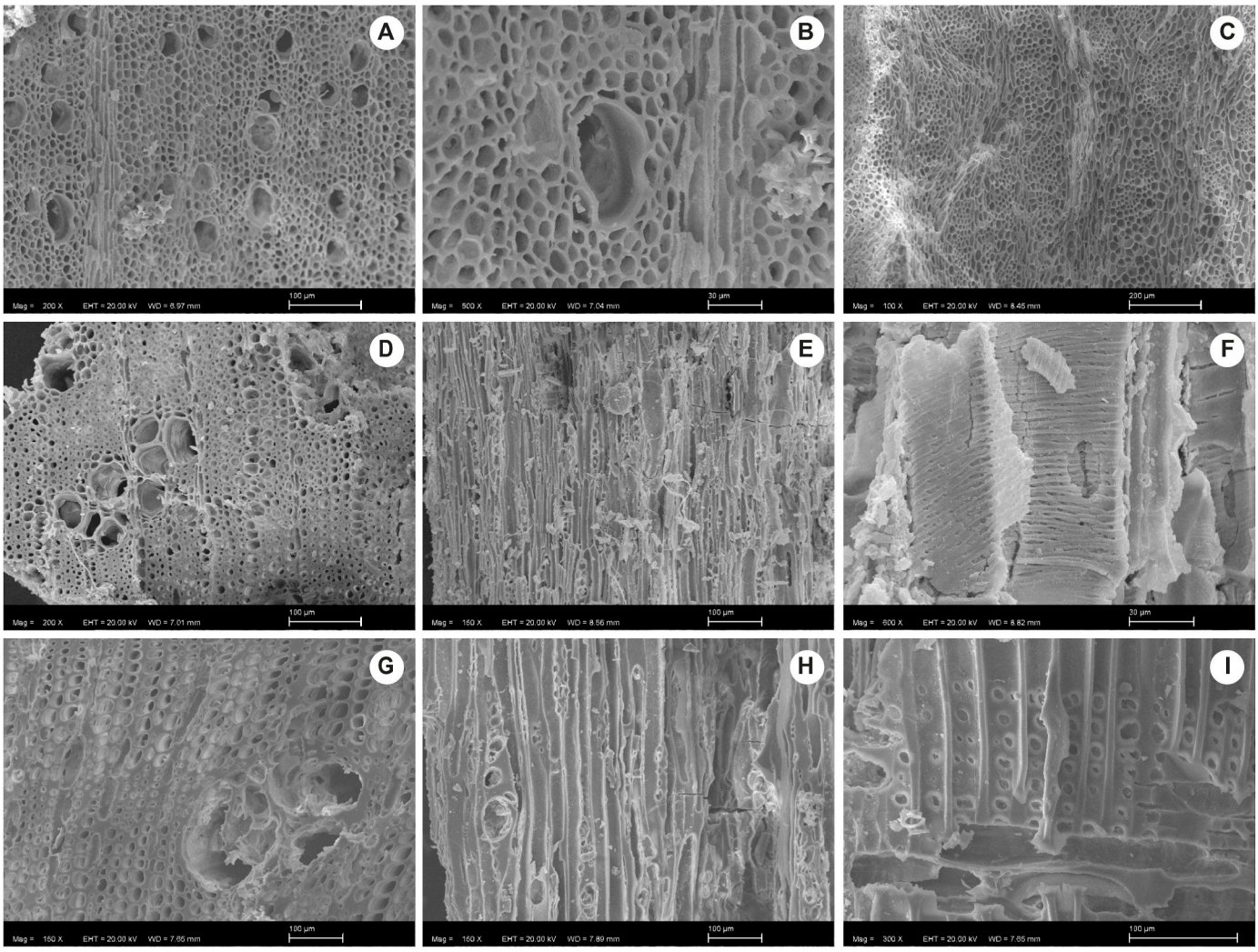

Fig. 7. SEM images of the taxa identified. A, *Erica arborea*, transversal section, HIC 18. B, *Erica arborea*, detail of the transversal section, HIC 18. C, *Erica arborea*, tangential section, HIC 22. D, Fabaceae, transversal section, HIC 21. E, Fabaceae, tangential section, HIC 21. F, Fabaceae, detail of vestured pits in vessels, tangential section, HIC 21. G, *Pinus canariensis*, transversal section, HIC 22. H, *Pinus canariensis*, tangential section, HIC 22. I, *Pinus canariensis*, radial section, HIC 22.

have been able to locate only the edifices Lomo Cabras (Id. 42) and Montaña de Orchilla (Id. 41), both in the NW rift.

The edifice of Lomo Cabras (Id. 42) yielded an age of 17 ± 1 ka (unspiked K-Ar). The age obtained indicates the youth of the lava, but it is possibly much younger, given the difficulty of applying the unspiked K-Ar method in recent basaltic lavas. It is isolated, the erosion and weathering degree is high compared to other Holocene lavas, and there is no evidence of a lava delta on the contemporary marine platform. However, remnants of a lava flow remain on the coastal cliff. Thus, we preliminarily place this eruption in the early Holocene, which would be the oldest edifice of those studied.

In Risica et al. (2022), sites HIE13, HIE14, HIE16, and HIE17 were considered together as Orchilla. However, sites HIE14, HIE16, and HIE17 belong to Montaña de Orchilla (Id. 41), whereas HIE13 corresponds to El Estacadero (Id. 27). The Montaña de Orchilla eruption was dated 8929 [9827, 7984] cal BP and El Estacadero 5661 [6583, 4785] cal BP. The event of La Hoya del Faro (Id. 29) is bracketed between both dates and, with this information, the Bayesian inference yields a date of 7390 [11004, 5503] cal BP.

Risica et al. (2022) interpreted the lava flows associated with the fissure of El Meridiano (Id. 16) as part of the Montaña de las Calcosas edifice (Id. 28). However, these lava flows postdate the edifice of Montaña de las Calcosas. As all paleomagnetic sampling sites attributed to Montaña de las Calcosas in that work were collected on lava flows from El Meridiano, the resulting date of 4138 [4619, 3676] cal BP was assigned to the latter (Table 2 and Suppl. Table S08). Montaña de las Calcosas event is constrained by forming a lava delta (<7000 yr) and being under the El Meridiano lava flows, and the model assigns a date of 5294 [8587, 3895] cal BP.

Sites HIE30, HIE31, HIE32, and HIE37, previously identified as Cuchillo del Roque (Risica et al., 2022), are now attributed to Roque de Basco (Id. 30) and have been dated to 5854 [6551, 5139] cal BP. Under these lava flows, we find the lavas of the Arenas Blancas (Id. 33) event, which formed a lava delta on the contemporaneous coastal platform, indicating an age of less than 7000 years BP. This bracketing provides a date of 6457 [8458, 5441] cal BP for Arenas Blancas.

Further reinterpretation was necessary for the Below Lomo Negro paleomagnetic sampling sites of Risica et al. (2022) (HIE26, HIE27, HIE28, and HIE29). Two of them (HIE27 and HIE29) correspond to Hoya del Verodal (Id. 25), and the other two (HIE26 and HIE28) to Montaña de los Guirres (Id. 24). The latter directly overlay Hoya del Verodal, indicating its proximity in time. The modeled ages according to this reinterpretation and the stratigraphic and geomorphic constraints resulted in an age of 5299 [5399, 5189] cal BP for Hoya del Verodal and 4872 [5379, 3845] cal BP for Montaña de los Guirres (Table 2).

The radiocarbon age and paleomagnetic data by Risica et al. (2022)

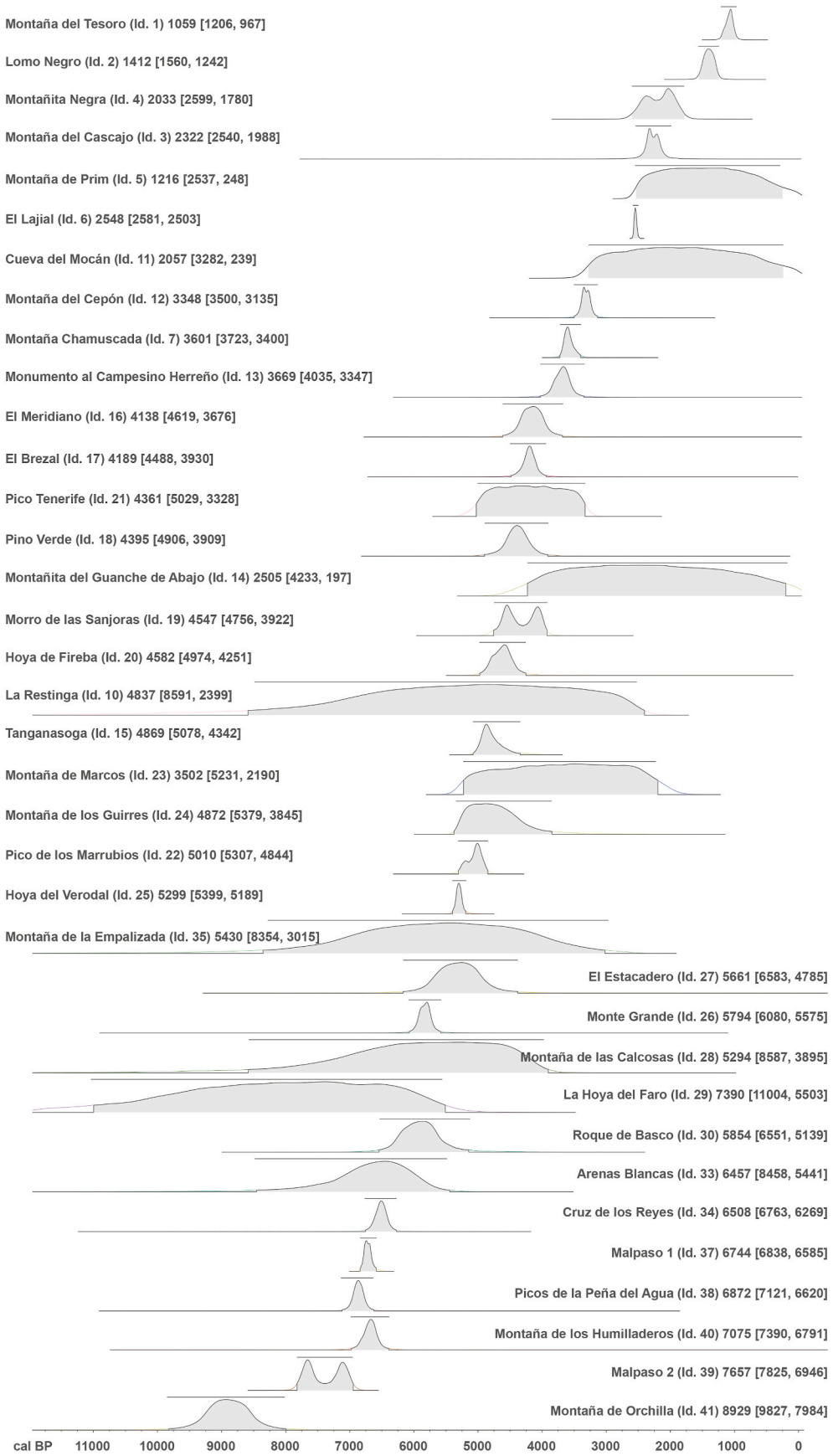

(caption on next page)

Fig. 8. Geochronological model of the Holocene volcanic history of El Hierro. Radiocarbon and paleomagnetic ages of the eruptive events allowed the estimate of the posterior distribution graphs for probability densities (curves) predicted by Bayesian inference in ChronoModel v. 3.2.7. The 95 % highest posterior density (HPD) regions are represented by the horizontal bars above the curves and by the grey filled areas under the curves. Labels: name of the eruption, mode of the posterior distribution (MAP), and 95 % highest posterior density (HPD) interval. Numerical results can be found in Table 2.

of Montañita Negra (Id. 4) provided a date of 2033 [2599, 1780] cal BP, i.e., the most recent date of the NW rift before Lomo Negro event.

The Lomo Negro (Id. 2) age has been the subject of a long debate (Hernández-Pacheco, 1982; Principe et al., 2020; Risica et al., 2022; Villasante-Marcos and Pavón-Carrasco, 2014). This eruption was related to a series of earthquakes on the island in 1793 (Hernández-Pacheco, 1982; Romero Ruiz, 2016). Villasante-Marcos and Pavón-Carrasco (2014) concluded that this eruption preceded 1793 and identified three possible paleomagnetic age ranges (2065–1943, 1540-1324, 451-348 BP). Risica et al. (2022) provided several possible paleomagnetic ages, some combining their data with the data of Villasante-Marcos and Pavón-Carrasco (2014). Moreover, a charcoal ^{14}C age was used to constrain these paleomagnetic ages, determining that the Lomo Negro eruption occurred in the sixteenth century CE. The recalibration of charcoal data from Risica et al. (2022) gave 463 [668, 173] cal BP (sample LOMO_NEGRO, Suppl. Table S11). This age is not plausible because, since 548-454 BP (1402–1496 CE), when the historical record began in the Canary Islands (Lobo Cabrera, 2019), there is no evidence of a subaerial eruption in El Hierro (Carracedo and Troll, 2016b; Guillén et al., 2023; Romero Ruiz, 2016). The Bayesian inference for Lomo Negro provided a date of 1412 [1560, 1242] cal BP. It is likely that the 1793 seismic crisis, which was so neatly described in historical documents, ended in a submarine eruption like the one recorded in 2011–2012.

This overview of the NW rift eruptions out of the island summit leaves two events, Sabinosa (Id. 32) and Charco Azul (Id. 31), of which we only know that they formed lava deltas on the contemporary coastal platform (i.e., <7000 years) and that they predate the historical record. Preliminarily and based on their degree of erosion and weathering, similar in both cases, we place their stratigraphic position as close to Arenas Blancas (Tables 1 and 2).

5.2. Rift S

The oldest eruptive events studied in the rift S are Calderetones (Id. 36) and Montaña de la Empalizada (Id. 35). The latter forms lava deltas (i.e., indicate <7000 years). Calderetones is isolated; consequently, the upper date is the beginning of the historical record. Instead, the lava flows of El Lajial overlap those of the Montaña de la Empalizada, delimiting their upper temporal limit. This bracketing provided a modeled date 5430 [95 % 8354, 3015] cal BP. The degree of erosion and weathering of Calderetones exceeds that of Montaña de la Empalizada. Therefore, it is in a stratigraphic position lower than Mt. de la Empalizada.

The Cueva del Mocán eruption (Id. 11) occurred in the transition zone towards the summit area, overlying the lava flows of Montaña del Cepón (Id. 12), dated to 3348 [3500, 3135] cal BP. This date and the lack of historical records for subaerial eruptions on El Hierro after 1496 bracketed this event for the Bayesian modeling, which provided a date of 2057 [3282, 239] cal BP. However, the absence of sediments between the two lava flows (Photo P16, Rodriguez-Gonzalez et al., 2024) suggests a much shorter time interval between eruptions than indicated by the respective MAPs. This feature suggests that the modeled date for Cueva del Mocán is likely biased towards the upper limit of the bracketing period (1496). Consequently, the Cueva del Mocán eruption was temporally positioned close to the Montaña del Cepón event (Tables 1 and 2).

Sites HIE01, HIE02, HIE03, HIE04, and HIE05, assigned to the Lajal eruption in Risica et al. (2022), actually belong to the El Lajial volcanic edifice (Id. 6), which is composed by Luna (HIE02), Roque Quemado (HIE04), Hoya del Roque (HIE01 and HIE05), and Aborigen (HIE03), among other construction episodes. Risica et al. (2022) considered the most likely age interval for the different construction episodes of the El Lajial edifice to be between 1428 and 1189 BP, according to paleomagnetic dating.

Besides, Risica et al. (2022) contributed the ^{14}C age of a shell (sample LAJ) from a marine sedimentary deposit that we interpret as a beachrock with volcanic clasts sourced from the lava flows of the Hoya del Roque episode of the El Lajial event. The combination of this ^{14}C age (LAJ) and paleomagnetic data of the five sites of El Lajial through the Bayesian inference yields the date of 2548 [2581, 2503] cal BP (Table 2).

Bimbape -or Bimbache- Culture was the manifestation of the island's first inhabitants. There is no definitive evidence of the first arrival of humans on the island of El Hierro, but recent dating points to the second century CE (Morales et al., 2023). One of the earliest radiocarbon datings yielded an age of ~1380-930 cal BP in the prehispanic settlement of Guinea (Jiménez González and Jiménez Gómez, 2007). Later ^{14}C dates gave 1520-1317 and 1510-1300 cal BP, dating barley seeds or *Visnea mocanera* fruits, respectively (Morales et al., 2017), and 1400-1306 cal BP, dating *Triticum* grain (Morales et al., 2023). The Bimbape culture collapsed in 1402 CE when the Normans conquered the island commanded by Jean de Bethencourt; previously, the island had undergone a demographic crisis due to mass slavery (Lobo Cabrera, 2019). On the El Lajial volcanic edifice, we have evidence of human occupation, including the use of volcanic caves as habitat (Cueva de Las Palomas, for instance), ceremonial areas, rock engraving sites, artifacts, and pottery spread across the lava field. The most solid evidence has been provided by recent and unpublished data from the archaeologists Consuelo Marrero and Valentín Barroso (Arqueocanarias S.L.) in Cueva de Los Saltos. They found an exceptional stratigraphy in this rock shelter of the Hoya del Roque episode lava flows, placed at 9 m a.s.l. and 200 m far from the coastline. During the excavation, they found a goat's horn at a level 70 cm deep, which provided a^{14}C date of 1652 [1885, 1478] cal BP (sample Rest-1, Suppl. Table S11). So, this ^{14}C date is among the oldest pieces of evidence for the human settlement on El Hierro Island and gives a minimal age for the El Lajial volcanic edifice, consistent with the estimated date of 2548 [2581, 2503] cal BP.

Lava flows of the La Restinga edifice (Id. 10) formed lava deltas, and El Lajial (Id. 6) lava flows overlaid some of them, bracketing this edifice between <7000 years and >2548 [2581, 2503] cal BP. These constraints resulted in a modeled date of 4837 [8591, 2399] cal BP. A dike of La Restinga was dated by ^{40}Ar/^{39}Ar (7 ± 2 ka, Becerril et al., 2016b). Despite the inconsistency of this dating method for the Holocene, the youth of this age is coherent with that time frame.

The most recent eruptive event of rift S is Montaña de Prim (Id. 5), which overlies La Restinga and El Lajial, indicating that this eruption was younger than the latter (<2548 [2581, 2503] cal BP). Once more, the upper date is the absence of historical subaerial eruptions in El Hierro since 1496. This bracketing yielded a date of 1216 [95 % 2537, 248] cal BP for Montaña de Prim.

5.3. Rift NE

The oldest events in the rift NE off the summit of the island appear to be Montaña de Aguarijo (Id. 9) and La Caleta (Id. 8). These eruptions are stratigraphically isolated and formed lava deltas on the contemporaneous coastal platform, i.e., are younger than 7000 years. The only age available is 18 ± 4 ka (unspiked K-Ar dating) for Montaña de Aguarijo, which is discarded by the geomorphic lower constraint of forming lava deltas. The close degree of erosion and weathering of both events with

Montaña Chamuscada allows us to place them in a stratigraphic position close to this eruption.

Several ages were published for the edifice of Montaña Chamuscada (Id. 7). Fuster et al. (1993) mentioned a ^{14}C age of 4230 BP without further detail. A later radiocarbon dating of a charred trunk within the lava flow gave an age of 2500 ± 70 BP (Guillou et al., 1996) (Suppl. S07). It corresponds to a charred trunk exceptionally preserved on a mold within a lava flow of this volcanic edifice (J. C. Carracedo, pers. comm., 2023). Risica et al. (2022) shift this eruption to the sixteenth century CE, considering as most likely their paleomagnetic interval of 454-421 BP due to its coincidence with their ^{14}C date of 466-306 cal BP. However, no evidence of a sixteenth-century onshore eruption on El Hierro has been found in the historical record (Carracedo and Troll, 2016a; Guillén et al., 2023; Lobo Cabrera, 2019; Romero Ruiz, 2016). Consequently, we discard both historical ages from Risica et al. (2022). The Bayesian inference applied to the three radiocarbon ages and the paleomagnetic interval of 3660-3395 BP (Suppl. S10) provided a date of 3601 [3723, 3400] cal BP (Table 2).

The edifice of Montaña del Tesoro (Id. 1) formed a lava delta on the coastal platform (Rodriguez-Gonzalez et al., 2022). The first attempt to date this eruption was made using unspiked K-Ar dating, which provided an age of 9 ± 6 ka (Rodriguez-Gonzalez et al., 2012). However, Risica et al. (2022) demonstrated that it was much younger by both ^{14}C and paleomagnetism. The geochronological model using the paleomagnetic interval of 740-915 AD and the radiocarbon age (1140 ± 30 BP, sample TES) provided a date of 1059 [1206, 967] cal BP for this edifice.

The Montaña del Cascajo eruption (Id. 3), previously dated by Becerril et al. (2016b) in 2350-2180 BP, provided a date with the geochronological model of 2322 [2540, 1988] cal BP.

5.4. Summit

This section discusses the 16 eruptions with vents at the island's summit (Table 1). Only four of them generated lava flows in addition to pyroclasts, and they are located in the transition zone towards the summit; Morro de las Sanjoras, El Brezal, Montaña del Cepón, and Tanganasoga (Table 1). The rest produced only pyroclastic deposits. Another characteristic feature is the occurrence of the two pumice deposits from Malpaso 1 and Malpaso 2, which are excellent stratigraphic markers (Figs. 4 and 5). The age of 14 of 16 involved volcanic edifices in this area was determined by radiocarbon dating. The remaining two events were bracketed temporally by stratigraphic constraints.

Malpaso 2 (Id. 39) and Montaña de los Humilladeros (Id. 40) are the precedents of extensive eruptive activity at the island's summit that lasted for 4500 years, from ca. 7800 to ca. 3200 cal BP (Table 2). The stratigraphic marker Malpaso 2 (Id. 39), with its vent location unknown, was dated 7657 [7825, 6946] cal BP and Montaña de los Humilladeros 7075 [7390, 6791] cal BP. Then, there was the eruption of Picos de la Peña del Agua 6872 [7121, 6620] cal BP (Id. 38).

The date of the Malpaso 1 (Id. 37) event is significant because its lower pumice unit is an excellent stratigraphic guide level at the island's summit. Furthermore, several hypotheses have been proposed for its vent, and its relationship with the El Golfo giant landslide has been controversial. This event is bracketed between the lower date of Malpaso 2 (7657 [7825, 6946] cal BP) and the upper date of the Pino Verde (Id. 18) event (4395 [4906, 3909] cal BP). Three of the six ages related to Malpaso 1 have been discarded for the geochronological model (samples Muestra núm. 2, HIC-01, and LOW_1; Suppl. Table S11). They are much older than the lower limit of Malpaso 2. This feature suggests the influence of magmatic CO_2 on these samples, which resulted in their apparent aging. The Bayesian inference with the other three ^{14}C ages provided the date 6744 [6838, 6585] cal BP.

The Malpaso 1 whitish pumice deposit and associated charcoals were already mentioned by Walter (1894). Malpaso 1 comprises a pyroclastic succession formed by two units (Figs. 4 and 5C-D and 6). The lower unit consists of a series of whitish-colored levels of millimetric to centimetric thickness composed of ash and lapilli with a maximum thickness that does not exceed 1 m. Pumice fragments from the coarser levels are characteristic. Pedrazzi et al. (2014) studied the stratigraphy of this lower unit in detail. The upper unit is formed by centimetric to decimetric levels of black lapilli, developing a sequence with a total thickness lower than 1 m. The Malpaso 1 deposits unconformably overlie a paleosol, sealing the pre-existing relief (Fig. 5C and D and 6). The lower pumice unit is interpreted as a laminated surge deposit (Balcells Herrera et al., 2010a; Gómez Sainz de Aja et al., 2010a; Pedrazzi et al., 2014), while the upper deposit is related to a tephra fall from a Strombolian eruption. The distribution of these deposits around the Pico de Malpaso suggests that the vent could be located at its summit.

About the relationship between the pumice unit of Malpaso 1 and the giant landslide of El Golfo, Pedrazzi et al. (2014) estimated that the age of this event must be equal to or younger than the age of the pumice deposit and postulated that possibly this eruptive event represented the final episode of the construction of the El Golfo composite volcano and could cause its giant landslide. This assumption was based on the fact that the deposits related to the Malpaso 1 are only found in the uppermost part of the El Golfo scar and not within the El Golfo embayment (see Fig. 2 in Pedrazzi et al., 2014). This assertion led Pedrazzi et al. (2014), without presenting any new dating, to question the ages of Pellicer (1977) and Perez-Torrado et al. (2011) for being too young and suggest that the charcoal used by Perez-Torrado et al. may derive from roots of younger plants burnt by forest fires or from younger deposits. Risica et al. (2022) obtained new ages, in agreement with Pellicer (1977) and Perez-Torrado et al. (2011), and refuted the pre-Holocene age suggested by Pedrazzi et al. (2014). Our results (Bayesian inference of radiocarbon ages of samples HIC-21, HIC-22, and UPP_1, and the ^{40}Ar/^{39}Ar age of sample HIR-156 of substratum lava) confirm the Holocene age for Malpaso 1 eruption. Furthermore, the anthracologic study supports the age by verifying that the HIC-22 charcoal corresponds to a branch fragment of *Erica arborea*. In the same way, the age of the El Golfo giant landslide must also be pre-Holocene, older than 18.9 ± 6.2 ka (^{40}Ar/^{39}Ar age of sample HIR-156), in agreement with other published age constraints (Guillou et al., 1996; Carracedo et al., 2001; Longpré et al., 2011).

After Malpaso 1 event, 12 eruptions occurred at the summit (Table 2). Six of these eruptions are underlaid by the Malpaso 1 pyroclastic deposits: Monumento al Campesino Herreño (Id. 13), Tanganasoga (Id. 15), El Brezal (Id. 17), Pino Verde (Id. 18), and Morro de las Sanjoras (Id. 19) (Table 1).

The Tanganasoga (Id. 15) is another controversial Holocene eruption at the island's summit. Tanganasoga is a complex stratovolcano edifice developed nested in the upper part of the El Golfo embayment giant landslide (e.g., Carracedo et al., 2001). The last activity developed several scoria cones along an N-S fissure and an a'a' lava field flowing downslope several kilometers northwards without reaching the coastline (Pellicer, 1977). Their pyroclastic fall deposits irregularly overlie the pre-existing eroded relief, being made up of lapilli, showing the particularity that the sequence culminates with large blocks (30–120 cm) of host rocks (Pellicer, 1977). The distinction between Malpaso 1 and Tanganasoga edifices was difficult (Pedrazzi et al., 2014; Pellicer, 1977; Perez-Torrado et al., 2011; Risica et al., 2022), but the identification of both sequences clarifies that most recent activity of Tanganasoga is later (4869 [5078, 4342] cal BP) and not related to Malpaso 1. The calibrated age of a sample from Pellicer (1977), Muestra No. 1, is consistent with this result (4705 [5351-4112] cal BP, Table S11). However, it was not included in the general model due to a lack of details on its location. Risica et al. (2022) mention other radiocarbon age (~4800–4700 BCE) for charcoal within the lapilli fallout attributed to the Tanganasoga. However, the lack of additional information does not allow the comparison, and it has not been included in the geochronological model.

6. Conclusions

New and revised multi-method dating data, supported by robust stratigraphic and geomorphic criteria, unravel the Holocene eruptive history of El Hierro Island. This study demonstrated that the anthracologic study of some charcoal samples before ^{14}C dating warrants the characteristics of dated materials, avoiding sterile discussions on the interpretation of results. Moreover, using multiple dating methods has proved to be an effective tool for determining the age of young volcanic deposits, with radiocarbon and paleomagnetism being the best approaches.

The reconstructed eruption history of El Hierro is more active than that reported earlier. This work confirms that El Hierro underwent at least 42 eruptive events during the Holocene. Eruptions were of Strombolian style, mostly combining explosive and effusive activity. However, the events on the highest part of the island's summit only generated pyroclastic deposits. We underline the role of the rifts in controlling the distribution of eruptive vents during the Holocene, as indicated by Carracedo et al. (2001) since 134 ka (the Rift volcanism).

The new chronostratigraphic reconstruction provides a higher frequency of eruptions, which indicates a significant volcanic hazard for El Hierro, according to the juvenile shield stage in which this oceanic volcanic island is developing.

Human presence on El Hierro since at least the fourth century has witnessed two subaerial eruptions, the probable submarine eruptions of 1721, 1777, and 1793, and the submarine event of 2011–2012 CE. This setting resulted in the widespread perception of a low volcanic risk among the inhabitants of El Hierro. Results are particularly relevant for elaborating on possible eruptive scenarios and defining the volcanic alert levels.

CRediT authorship contribution statement

C. Prieto-Torrell: Writing – review & editing, Writing – original draft, Visualization, Validation, Supervision, Methodology, Investigation, Formal analysis, Conceptualization. **J.L. Fernandez-Turiel:** Writing – review & editing, Writing – original draft, Visualization, Validation, Resources, Project administration, Methodology, Investigation, Funding acquisition, Formal analysis, Data curation, Conceptualization. **A. Rodriguez-Gonzalez:** Writing – review & editing, Writing – original draft, Visualization, Validation, Resources, Methodology, Investigation, Funding acquisition, Formal analysis, Data curation, Conceptualization. **M. Aulinas:** Writing – review & editing, Investigation. **E. Beamud:** Writing – review & editing, Visualization, Methodology, Investigation, Formal analysis. **M.C. Cabrera:** Writing – review & editing, Investigation. **C. Criado:** Writing – review & editing, Investigation. **H. Guillou:** Writing – review & editing, Visualization, Methodology, Investigation, Formal analysis. **P. Vidal-Matutano:** Writing – review & editing, Visualization, Methodology, Investigation, Formal analysis. **F.J. Perez-Torrado:** Writing – review & editing, Writing – original draft, Visualization, Validation, Resources, Project administration, Methodology, Investigation, Funding acquisition, Formal analysis, Data curation, Conceptualization.

Declaration of competing interest

The authors declare that they have no known competing financial interests or personal relationships that could have appeared to influence the work reported in this paper.

Acknowledgments

Financial support was provided by Grant PGC2018-101027-B-I00, funded by MCIN/AEI/10.13039/501100011033 and by ERDF 'A way of making Europe'. CPT acknowledges the Ph.D. grant 2021 FISDU 00347 funded by the Departament de Recerca i Universitats de la Generalitat de Catalunya. PVM is a beneficiary of an IJC2020-043481-I Grant funded by MCIN/AEI/10.13039/501100011033 and by 'European Union NextGenerationEU/PRTR'. SEM pictures of charcoal fragments were funded by the research project PID2021-125055NA-I00 granted by MCIN/AEI/10.13039/501100011033 and by ERDF 'A way of making Europe'. This study was carried out in the Research Consolidated Groups GEOVOL (Canary Islands Government, ULPGC) and Structure and Dynamics of the Earth (Generalitat de Catalunya, 2021 SGR 00413). We are grateful to the Cabildo de El Hierro and El Hierro UNESCO Global Geopark for permission to access the geopark. Thanks to the archaeologists Consuelo Marrero and Valentín Barroso (Arqueocanarias S.L.) for facilitating the dating of Cueva de Los Saltos. We want to express our gratitude to the editor Pierre-Henri Blard for handling our manuscript. We also thank the reviewers for their valuable comments and suggestions, which significantly improved our work.

Appendix A. Supplementary data

Supplementary data to this article can be found online at https://doi.org/10.1016/j.quageo.2025.101685.

Data availability

Data are included in the submission

References

Abdel-Monem, A., Watkins, N.D., Gast, P.W., 1972. Potassium-argon ages, volcanic stratigraphy, and geomagnetic polarity history of the Canary Islands; Tenerife, La Palma and Hierro. Am. J. Sci. 272, 805–825. https://doi.org/10.2475/ajs.272.9.805.

Abis, C., Dajma, F., Di Capua, A., Martì Molist, J., Meletlidis, S., Norini, G., Principe, C., Groppelli, G., 2023. Geology of El Hierro Southern Rift, Canary Islands, Spain. J. Maps 1–15. https://doi.org/10.1080/17445647.2023.2214173.

Acosta, J., Uchupi, E., Smith, D., Muñoz, A., Herranz, P., Palomo, C., Llanes, P., Ballesteros, M., 2005. Comparison of volcanic rifts on La Palma and El Hierro, Canary Islands and the island of Hawaii. In: Clift, P., Acosta, Juan (Eds.), Geophysics of the Canary Islands: Results of Spain's Exclusive Economic Zone Program. Springer, Netherlands, Dordrecht, pp. 59–90. https://doi.org/10.1007/1-4020-4352-X_3.

AEMET, 2012. Climate atlas of the archipelagos of the Canary Islands, Madeira and the Azores, air temperature and precipitation (1971-2000). Agencia Estatal de Meteorología. Ministerio de Agricultura, Alimentación y Medio Ambiente.

Alva-Valdivia, L.M., Rodríguez-Trejo, A., Morales, J., González-Rangel, J.A., Agarwal, A., 2019. Paleomagnetism and age constraints of historical lava flows from the El Jorullo volcano, Michoacán, Mexico. J. S. Am. Earth Sci. 93, 439–448. https://doi.org/10.1016/j.jsames.2019.05.016.

Balcells Herrera, R., Gómez Sainz de Aja, J.A., Pineda Velasco, A., 2010a. Mapa geológico de España Escala 1:25.000, Sabinosa (Isla de El Hierro), Hoja 1105-III. IGME. Segunda Serie (MAGNA).

Balcells Herrera, R., Gómez Sainz de Aja, J.A., Pineda Velasco, A., 2010b. Mapa geológico de España escala 1:25.000, La Restinga (Isla de El Hierro). Hoja 1108-II/I. IGME, Segunda Serie (MAGNA).

Becerril, L., Bartolini, S., Sobradelo, R., Martí, J., Morales, J.M., Galindo, I., 2014. Long-term volcanic hazard assessment on El Hierro (Canary Islands). Nat. Hazards Earth Syst. Sci. 14, 1853–1870. https://doi.org/10.5194/nhess-14-1853-2014.

Becerril, L., Cappello, A., Galindo, I., Neri, M., Del Negro, C., 2013. Spatial probability distribution of future volcanic eruptions at El Hierro island (Canary Islands, Spain). J. Volcanol. Geoth. Res. 257, 21–30. https://doi.org/10.1016/j.jvolgeores.2013.03.005.

Becerril, L., Galve, J.P., Morales, J.M., Romero, C., Sánchez, N., Martí, J., Galindo, I., 2016a. Volcano-Structure of El Hierro (Canary Islands). J. Maps 12, 43–52. https://doi.org/10.1080/17445647.2016.1157767.

Becerril, L., Ubide, T., Sudo, M., Martí, J., Galindo, I., Galé, C., Morales, J.M., Yepes, J., Lago, M., 2016b. Geochronological constraints on the evolution of El Hierro (Canary Islands). J. Afr. Earth Sci. 113, 88–94. https://doi.org/10.1016/j.jafrearsci.2015.10.012.

Bonadonna, C., Pistolesi, M., Biass, S., Voloschina, M., Romero, J., Coppola, D., Folch, A., D'Auria, L., Martin-Lorenzo, A., Dominguez, L., Pastore, C., Reyes Hardy, M.-P., Rodríguez, F., 2022. Physical characterization of long-lasting hybrid eruptions: the 2021 Tajogaite eruption of Cumbre Vieja (La Palma, Canary Islands). J. Geophys. Res. Solid Earth 127, e2022JB025302. https://doi.org/10.1029/2022JB025302.

Carracedo, J.C., 1999. Growth, structure, instability and collapse of Canarian volcanoes and comparisons with Hawaiian volcanoes. J. Volcanol. Geoth. Res. 94, 1–19. https://doi.org/10.1016/S0377-0273(99)00095-5.

Carracedo, J.C., 1996. A Simple Model for the Genesis of Large Gravitational Landslide Hazards in the Canary Islands, vol 110. Geological Society, London, Special Publications, p. 125. https://doi.org/10.1144/GSL.SP.1996.110.01.10.

Carracedo, J.C., 1994. The Canary Islands: an example of structural control on the growth of large oceanic-island volcanoes. J. Volcanol. Geoth. Res. 60, 225–241. https://doi.org/10.1016/0377-0273(94)90053-1.
Carracedo, J.C., Badiola, E.R., Guillou, H., de la Nuez, J., Pérez Torrado, F.J., 2001. Geology and volcanology of La Palma and El Hierro, western Canaries. Estud. Geol. 57, 175–273. https://doi.org/10.3989/egeol.01575-6134.
Carracedo, J.-C., Perez-Torrado, F.-J., Rodriguez-Gonzalez, A., Fernandez-Turiel, J.-L., Klügel, A., Troll, V.R., Wiesmaier, S., 2012a. The ongoing volcanic eruption of El Hierro, Canary Islands. Eos, Transact. America Geophys. Union 93, 89–90. https://doi.org/10.1029/2012EO090002.
Carracedo, J.C., Rodríguez Badiola, E., Guillou, H., Paterne, M., Scaillet, S., Torrado, F.J. P., Paris, R., Fra-Paleo, U., Hansen, A., 2007. Eruptive and structural history of Teide volcano and rift zones of Tenerife, Canary Islands. GSA Bulletin 119, 1027–1051. https://doi.org/10.1130/B26087.1.
Carracedo, J.-C., Torrado, F.P., González, A.R., Soler, V., Fernandez-Turiel, J.-L., Troll, V. R., Wiesmaier, S., 2012b. The 2011 submarine volcanic eruption in El Hierro (Canary Islands). Geol. Today 28, 53–58. https://doi.org/10.1111/j.1365-2451.2012.00827.x.
Carracedo, J.C., Troll, V., 2021. North-east Atlantic islands: the Macaronesian archipelagos. In: Alderton, D., Elias, S.A. (Eds.), Encyclopedia of Geology, second ed. Elsevier, pp. 674–699.
Carracedo, J.C., Troll, V.R., 2016a. The Canary Islands: an introduction. In: Troll, V.R., Carracedo, J.C. (Eds.), The Geology of the Canary Islands. Elsevier, pp. 1–41. https://doi.org/10.1016/B978-0-12-809663-5.00001-3.
Carracedo, J.C., Troll, V.R., 2016b. The geology of El Hierro. In: Troll, V.R., Carracedo, J. C. (Eds.), The Geology of the Canary Islands. Elsevier, pp. 43–99. https://doi.org/10.1016/B978-0-12-809663-5.00002-5.
Carracedo, J.C., Troll, V.R., Day, J.M., Geiger, H., Aulinas, M., Soler, V., Deegan, F.M., Perez-Torrado, F.J., Gisbert, G., Gazel, E., 2022. The 2021 eruption of the Cumbre Vieja volcanic ridge on La Palma, Canary Islands. Geol. Today 38, 94–107.
Carracedo, J.C., Troll, V.R., Zaczek, K., Rodríguez-González, A., Soler, V., Deegan, F.M., 2015. The 2011–2012 submarine eruption off El Hierro, Canary Islands: new lessons in oceanic island growth and volcanic crisis management. Earth Sci. Rev. 150, 168–200. https://doi.org/10.1016/j.earscirev.2015.06.007.
Clague, D.A., Sherrod, D.R., 2014. Growth and degradation of Hawaiian volcanoes. In: Characteristics of Hawaiian Volcanoes. U.S. Geological Survey Professional Paper, pp. 97–146.
del Arco Aguilar, M.-J., González-González, R., Garzón-Machado, V., Pizarro-Hernández, B., 2010. Actual and potential natural vegetation on the Canary Islands and its conservation status. Biodivers. Conserv. 19, 3089–3140. https://doi.org/10.1007/s10531-010-9881-2.
Fuster, J.M., Hernan, F., Cendrero, A., Coello, J., Cantagrel, J.M., Ancochea, E., Ibarrola, E., 1993. Geocronología de la isla de El Hierro (Islas Canarias). Bol. R. Soc. Esp. Hist. Nat. 88, 85–97.
Gee, M.J.R., Watts, A.B., Masson, D.G., Mitchell, N.C., 2001. Landslides and the evolution of El Hierro in the Canary Islands. Mar. Geol. 177, 271–293. https://doi.org/10.1016/S0025-3227(01)00153-0.
Geldmacher, J., Hoernle, K., Bogaard, P.v. d., Duggen, S., Werner, R., 2005. New 40Ar/39Ar age and geochemical data from seamounts in the Canary and Madeira volcanic provinces: support for the mantle plume hypothesis. Earth Planet Sci. Lett. 237, 85–101. https://doi.org/10.1016/j.epsl.2005.04.037.
Gómez Sainz de Aja, J.A., Balcells Herrera, R., Pineda Velasco, A., 2010a. Mapa geológico de España escala 1:25.000, Frontera (Isla de El Hierro). Hoja 1105-IV. IGME, Segunda Serie (MAGNA).
Gómez Sainz de Aja, J.A., Balcells Herrera, R., Pineda Velasco, A., 2010b. Mapa geológico de España Escala 1:25.000, Valverde (Isla de El Hierro). Hoja 1105-II. IGME, Segunda Serie (MAGNA).
Guilbaud, M.-N., Alcalá-Reygosa, J., Schimmelpfennig, I., Arce, J.L., 2022. Testing less-conventional methods to date a late-pleistocene to Holocene eruption: radiocarbon dating of paleosols and 36Cl exposure ages at Pelado volcano, Sierra Chichinautzin, Central Mexico. Quat. Geochronol. 68, 101252. https://doi.org/10.1016/j.quageo.2022.101252.
Guillén, C., Romero, M.C., Galindo, I., 2023. Review of submarine eruptions in El Hierro prior to Tagoro. In: González, P.J. (Ed.), El Hierro Island. Springer International Publishing, Cham, pp. 41–58. https://doi.org/10.1007/978-3-031-35135-8_3.
Guillou, H., Carracedo, J.C., Day, S.J., 1998. Dating of the Upper Pleistocene–Holocene volcanic activity of La Palma using the unspiked K–Ar technique. J. Volcanol. Geoth. Res. 86, 137–149. https://doi.org/10.1016/S0377-0273(98)00074-2.
Guillou, H., Carracedo, J.C., Pérez Torrado, F.J., Rodríguez Badiola, E., 1996. K-Ar ages and magnetic stratigraphy of a hotspot-induced, fast grown oceanic island: El Hierro, Canary Islands. J. Volcanol. Geoth. Res. 73, 141–155. https://doi.org/10.1016/0377-0273(96)00021-2.
Guillou, H., Nomade, S., Carracedo, J.C., Kissel, C., Laj, C., Perez Torrado, F.J., Wandres, C., 2011. Effectiveness of combined unspiked K–Ar and 40Ar/39Ar dating methods in the 14C age range. Quat. Geochronol. 6, 530–538. https://doi.org/10.1016/j.quageo.2011.03.011.
Hatté, C., Jull, A.J.T., 2025. 14C dating of plant macrofossils. In: Elias, S. (Ed.), Encyclopedia of Quaternary Science, third ed. Elsevier, Oxford, pp. 608–617. https://doi.org/10.1016/B978-0-323-99931-1.00075-1.
Heaton, T.J., Köhler, P., Butzin, M., Bard, E., Reimer, R.W., Austin, W.E.N., Bronk Ramsey, C., Grootes, P.M., Hughen, K.A., Kromer, B., Reimer, P.J., Adkins, J., Burke, A., Cook, M.S., Olsen, J., Skinner, L.C., 2020. Marine20—the marine radiocarbon age calibration curve (0–55,000 cal BP). Radiocarbon 62, 779–820. https://doi.org/10.1017/RDC.2020.68.
Hernández-Pacheco, A., 1982. Sobre una posible erupción en 1793 en la isla de El Hierro (Canarias). Estud. Geol. 38, 15–26.
Hoernle, K., Schmincke, H.U., 1993. The role of partial melting in the 15-Ma geochemical evolution of Gran Canaria: a blob model for the Canary hotspot. J. Petrol. 34, 599–626. https://doi.org/10.1093/petrology/34.3.599.
Holdaway, R.N., Duffy, B., Kennedy, B., 2018. Evidence for magmatic carbon bias in 14C dating of the Taupo and other major eruptions. Nat. Commun. 9, 4110. https://doi.org/10.1038/s41467-018-06357-0.
ISTAC, 2023. Estadísticas por temas. http://www.gobiernodecanarias.org/istac/ accessed 1.23.23.
Jiménez González, V.I., Jiménez Gómez, M.C., 2007. Dataciones radiocarbónicas del asentamiento de Guinea (Frontera). El Hierro, Canarias. Veleia 24–25, 1235–1244.
Kämmer, F., 1976. The influence of man on the vegetation of the island of Hierro (Canary Islands). In: Kunkel, G. (Ed.), Biogeography and Ecology in the Canary Islands. Springer, Netherlands, Dordrecht, pp. 327–346. https://doi.org/10.1007/978-94-010-1566-0_12.
Klimeš, J., Hussain, Y., Mreyen, A.-S., Cauchie, L., Schlögel, R., Piroton, V., Petružálek, M., Blahůt, J., René, M., Meletlidis, S., Havenith, H.-B., 2023. New insights into the internal structures and geotechnical rock properties of the giant San Andrés landslide, El Hierro Island, Spain. Remote Sens. 15. https://doi.org/10.3390/rs15061627.
Lanos, P., 2004. Bayesian inference of calibration curves: application to archaeomagnetism. In: Buck, C.E., Millard, A.R. (Eds.), Tools for Constructing Chronologies: Crossing Disciplinary Boundaries. Springer, London, London, pp. 43–82. https://doi.org/10.1007/978-1-4471-0231-1_3.
Lanos, Ph, Dufresne, Ph, 2024. ChronoModel Version 3: Software for Chronological Modeling of Archaeological Data Using Bayesian Statistics. CNRS.
Lanos, Ph, Dufresne, Ph, 2023. ChronoModel Version 3: Software for Chronological Modeling of Archaeological Data Using Bayesian Statistics.
Lanos, P., Philippe, A., 2017. Hierarchical Bayesian modeling for combining dates in archeological context. Journal de la société française de statistique 158, 72–88.
Lanos, Ph., Philippe, A., 2018. Event date model: a robust bayesian tool for chronology building. Commun. Stat. Appl. Methods 25, 131–157.
Le Bas, M.J., Le Maitre, R.W., Streckeisen, A., Zanettin, B., IUGS Subcommission on the Systematics of Igneous Rocks, 1986. A chemical classification of volcanic rocks based on the total alkali-silica diagram. J. Petrol. 27, 745–750. https://doi.org/10.1093/petrology/27.3.745.
Lerner, G.A., Piispa, E.J., Bowles, J.A., Ort, M.H., 2022. Paleomagnetism and rock magnetism as tools for volcanology. Bull. Volcanol. 84, 24. https://doi.org/10.1007/s00445-022-01529-9.
Lobo Cabrera, M., 2019. El Hierro. De la Prehistoria a la Colonización. Mercurio Editorial.
Lockwood, J.P., Lipman, P.W., 1987. Holocene eruptive history of Mauna Loa volcano. Volcan. Hawaii 1, 509–535.
Longpré, M.-A., Chadwick, J.P., Wijbrans, J., Iping, R., 2011. Age of the El Golfo debris avalanche, El Hierro (Canary Islands): new constraints from laser and furnace 40Ar/39Ar dating. J. Volcanol. Geoth. Res. 203, 76–80. https://doi.org/10.1016/j.jvolgeores.2011.04.002.
Mahgoub, A.N., Böhnel, H., Siebe, C., Salinas, S., Guilbaud, M.-N., 2017. Paleomagnetically inferred ages of a cluster of Holocene monogenetic eruptions in the Tacámbaro-Puruarán area (Michoacán, México): implications for volcanic hazards. J. Volcanol. Geoth. Res. 347, 360–370. https://doi.org/10.1016/j.jvolgeores.2017.10.004.
Malaguti, A.B., Rosi, M., Pistolesi, M., Speranza, F., Menzies, M., 2021. The contribution of palaeomagnetism, tephrochronology and radiocarbon dating to refine the last 1100 years of eruptive activity at Vulcano (Italy). Bull. Volcanol. 84, 12. https://doi.org/10.1007/s00445-021-01515-7.
Masson, D.G., Watts, A.B., Gee, M.J.R., Urgeles, R., Mitchell, N.C., Le Bas, T.P., Canals, M., 2002. Slope failures on the flanks of the western Canary Islands. Earth Sci. Rev. 57, 1–35. https://doi.org/10.1016/S0012-8252(01)00069-1.
Meletlidis, S., Becerril, L., Felpeto, A., 2023. Past, present and future volcanic activity on El Hierro. In: González, P.J. (Ed.), El Hierro Island. Springer International Publishing, Cham, pp. 17–39. https://doi.org/10.1007/978-3-031-35135-8_2.
Meletlidis Tsiogalos, S., 2017. Eruptive Dynamics and Petrological Evolution of Recent Volcanism on the El Hierro Island, Implications for Volcanic Hazard Assessment (PhD Thesis). Universitat de Barcelona, Barcelona.
Meteoblue, 2024. Simulated historical climate & weather data for El Hierro. https://www.meteoblue.com/en/weather/historyclimate/climatemodelled/el-hierro_spain_2516747 accessed 4.12.24.
Montagnoli, A., Chiatante, D., Dimitrova, A., Terzaghi, M., Pinto, J.R., Dumroese, R.K., 2021. Early pine root anatomy and primary and lateral root formation are affected by container size: implications in dry-summer climates. Reforesta 12, 20–34. https://doi.org/10.21750/REFOR.12.04.96.
Morales, J., Rodríguez, A., Henríquez-Valido, P., Fernández Eraso, J., Mujika Alustiza, J. A., Arrizabalaga Valbuena, Á., García Díez, M., 2017. Agricultura y recolección vegetal en la arqueología prehispánica de las Islas Canarias (siglos III-XV d.C.): la contribución de los estudios carpológicos. In: Miscelánea En Homenaje a Lydia Zapata Peña (1965-2015). Universidad del País Vasco, Bilbao, pp. 189–217.
Morales, J., Speciale, C., Rodríguez-Rodríguez, A., Henríquez-Valido, P., Marrero-Salas, E., Hernández-Marrero, J.C., López, R., Delgado-Darias, T., Hagenblad, J., Fregel, R., Santana, J., 2023. Agriculture and crop dispersal in the western periphery of the Old World: the Amazigh/Berber settling of the Canary Islands (ca. 2nd–15th centuries CE). Veg. Hist. Archaeobotany. https://doi.org/10.1007/s00334-023-00920-6.
Nitta, H., Saito, T., Shitaoka, Y., 2020. Recent eruption history inferred from eruption ages of the two latest lava flows using multi-dating at Yokodake Volcano, Japan. Earth Planets Space 72, 103. https://doi.org/10.1186/s40623-020-01220-3.

Pardo-Gordó, S., González Marrero, M. del C., Vidal Matutano, P., Rodríguez Rodríguez, A., 2022. Dating prehispanic and colonial sites on the island of Gran Canaria: a proposal for a radiocarbon hygiene protocol. Revista Tabona 22, 435–459. https://doi.org/10.25145/j.tabona.2022.22.22.

Pavón-Carrasco, FcoJ., Rodríguez-González, J., Osete, M.L., Torta, J.M., 2011. A Matlab tool for archaeomagnetic dating. J. Archaeol. Sci. 38, 408–419. https://doi.org/10.1016/j.jas.2010.09.021.

Pasquier-Cardin, A., Allard, P., Ferreira, T., Hatte, C., Coutinho, R., Fontugne, M., Jaudon, M., 1999. Magma-derived CO2 emissions recorded in 14C and 13C content of plants growing in Furnas caldera, Azores. J. Volcanol. Geotherm. Res. 92, 195–207. https://doi.org/10.1016/S0377-0273(99)00076-1.

Pavón-Carrasco, F.J., Osete, M.L., Torta, J.M., De Santis, A., 2014. A geomagnetic field model for the Holocene based on archaeomagnetic and lava flow data. Earth Planet Sci. Lett. 388, 98–109. https://doi.org/10.1016/j.epsl.2013.11.046.

Pedrazzi, D., Becerril, L., Martí, J., Meletlidis, S., Galindo, I., 2014. Explosive felsic volcanism on El Hierro (Canary Islands). Bull. Volcanol. 76, 863. https://doi.org/10.1007/s00445-014-0863-1.

Pellicer, M.J., 1977. Estudio volcanológico de la Isla de El Hierro (Islas Canarias). Estud. Geol. 33, 181–197.

Pérez de Paz, L., del Arco, M., Wildpret, W., 1981. Contribución al conocimiento de la flora y vegetación de El Hierro (Islas Canarias) I. Lagascalia 10, 23–57.

Perez-Torrado, F., Carracedo, J., Rodriguez-Gonzalez, A., Soler, V., Troll, V., Wiesmaier, S., 2012. The submarine eruption of La Restinga (El Hierro, Canary Islands): October 2011-March 2012. Estud. Geol. 68, 5–27. https://doi.org/10.3989/egeol.40918.179.

Perez-Torrado, F.J., Rodriguez-Gonzalez, A., Carracedo, J.C., Fernandez-Turiel, J.L., Guillou, H., Hansen, A., Rodriguez Badiola, E., 2011. Edades C-14 del Rift ONO de El Hierro (Islas Canarias). Presented at the El Cuaternario en España y Áreas Afines, Avances en 2011, Asociación Española para el Estudio del Cuaternario (AEQUA), pp. 101–104. Andorra la Vella.

Peterson, C.A., Enstone, D.E., Taylor, J.H., 1999. Pine root structure and its potential significance for root function. Plant Soil 217, 205–213. https://doi.org/10.1023/A:1004668522795.

Pressling, N., Trusdell, F.A., Gubbins, D., 2009. New and revised 14C dates for Hawaiian surface lava flows: paleomagnetic and geomagnetic implications. Geophys. Res. Lett. 36. https://doi.org/10.1029/2009GL037792.

Prieto-Torrell, C., Albert, H., Aulinas, M., González-Esvertit, E., Arienzo, I., Gisbert, G., Troll, V.R., Fernandez-Turiel, J.-L., Rodriguez-Gonzalez, A., Perez-Torrado, F.-J., 2025. Mush system heterogeneities control magma composition and eruptive style on the Ocean Island of El Hierro, Canary Islands. Contrib. Mineral. Petrol. 180, 32. https://doi.org/10.1007/s00410-025-02216-6.

Prieto-Torrell, C., Aulinas, M., Cabrera, M.C., Criado, C., Fernandez-Turiel, J.-L., Perez-Torrado, F.-J., Rodriguez-Gonzalez, A., 2024. Petrographic dataset of the Holocene volcanism on the island of El Hierro (Canary Islands, Spain). https://doi.org/10.20420/1763.2024.663.

Prieto-Torrell, C., Rodriguez-Gonzalez, A., Aulinas, M., Fernandez-Turiel, J.L., Cabrera, M.C., Criado, C., Perez-Torrado, F.J., 2021. Modelling and simulation of a lava flow affecting a shore platform: a case study of Montaña de Aguarijo eruption, El Hierro (Canary Islands, Spain). J. Maps 17, 502–511. https://doi.org/10.1080/17445647.2021.1972853.

Principe, C., Meletlidis, S., Giordano, D., Kolzenburg, S., La Felice, S., Gogichaishvili, A., Devidze, M., Cejudo, R., Groppelli, G., Dingwell, D.B., Marti Molist, J., 2020. Lomo Negro (El Hierro) – geology, archaeomagnetic dating and emplacement dynamics of a "monogenetic" eruption. Presented at the IAVCEI - 8th International Maar Conference, Petropavlovsk-Kamchatsky, Russia, pp. 48–49.

Reimer, P.J., Austin, W.E.N., Bard, E., Bayliss, A., Blackwell, P.G., Bronk Ramsey, C., Butzin, M., Cheng, H., Edwards, R.L., Friedrich, M., Grootes, P.M., Guilderson, T.P., Hajdas, I., Heaton, T.J., Hogg, A.G., Hughen, K.A., Kromer, B., Manning, S.W., Muscheler, R., Palmer, J.G., Pearson, C., van der Plicht, J., Reimer, R.W., Richards, D.A., Scott, E.M., Southon, J.R., Turney, C.S.M., Wacker, L., Adolphi, F., Büntgen, U., Capano, M., Fahrni, S.M., Fogtmann-Schulz, A., Friedrich, R., Köhler, P., Kudsk, S., Miyake, F., Olsen, J., Reinig, F., Sakamoto, M., Sookdeo, A., Talamo, S., 2020. The IntCal20 Northern Hemisphere radiocarbon age calibration curve (0–55 cal kBP). Radiocarbon 62, 725–757. https://doi.org/10.1017/RDC.2020.41.

Risica, G., Di Roberto, A., Speranza, F., Carlo, P.D., Pompilio, M., Meletlidis, S., Todrani, A., 2022. Reconstruction of the subaerial Holocene volcanic activity through paleomagnetic and 14C dating methods: El Hierro (Canary Islands). J. Volcanol. Geoth. Res. 425, 107526. https://doi.org/10.1016/j.jvolgeores.2022.107526.

Risica, G., Di Roberto, A., Speranza, F., Del Carlo, P., Pompilio, M., Meletlidis, S., Rosi, M., 2020. Refining the Holocene eruptive activity at Tenerife (Canary Islands): the contribution of palaeomagnetism. J. Volcanol. Geoth. Res. 401, 106930. https://doi.org/10.1016/j.jvolgeores.2020.106930.

Rivas Martínez, S., 1987. Memoria del mapa de series de vegetación de España 1: 400.000. ICONA. Ministerio de Agricultura, Pesca y Alimentación, Madrid.

Rodriguez-Gonzalez, A., Fernandez-Turiel, J.L., Aulinas, M., Cabrera, M.C., Prieto-Torrell, C., Rodriguez, G.A., Guillou, H., Perez-Torrado, F.J., 2022. Lava deltas, a key landform in oceanic volcanic islands: El Hierro, Canary Islands. Geomorphology 416, 108427. https://doi.org/10.1016/j.geomorph.2022.108427.

Rodriguez-Gonzalez, A., Fernandez-Turiel, J.-L., Cabrera Santana, M.C., Criado, C., Prieto-Torrell, C., Aulinas, M., Perez-Torrado, F.-J., 2024. Image dataset of the Holocene volcanism on the island of El Hierro (canary island, Spain): stratigraphic relationships. https://doi.org/10.20420/1770.2024.695.

Rodriguez-Gonzalez, A., Fernandez-Turiel, J.L., Perez-Torrado, F.J., Hansen, A., Aulinas, M., Carracedo, J.C., Gimeno, D., Guillou, H., Paris, R., Paterne, M., 2009. The Holocene volcanic history of Gran Canaria island: implications for volcanic hazards. J. Quat. Sci. 24, 697–709. https://doi.org/10.1002/jqs.1294.

Rodriguez-Gonzalez, A., Perez-Torrado, F.J., Fernandez-Turiel, J.L., Carracedo, J.C., Guillou, H., 2012. Modelado geomorfológico con técnicas SIG de erupciones volcánicas generadoras de plataformas costeras: el volcán de Montaña del Tesoro (El Hierro, Islas Canarias). In: Geotemas. Presented at the VIII Congreso Geológico de España, Oviedo, p. 4. CD 07-265.

Romero Ruiz, C., 2016. Historias de volcanes. Isla de El Hierro. In: Arozena Concepción, M.E., Romero Ruiz, C. (Eds.), Temas y Lugares: Homenaje a Eduardo Martínez de Pisón. Servicio de Publicaciones, Universidad de La Laguna, La Laguna, Santa Cruz de Tenerife, pp. 327–373.

Rufer, D., Gnos, E., Mettier, R., Preusser, F., Schreurs, G., 2011. Proposing new approaches for dating young volcanic eruptions by luminescence methods. Geochronometria 39, 48–56. https://doi.org/10.2478/s13386-011-0049-y.

Santana, J., del Pino, M., Morales, J., Fregel, R., Hagenblad, J., Morquecho, A., Brito-Mayor, A., Henríquez, P., Jiménez, J., Serrano, J.G., Sánchez-Cañadillas, E., Ordóñez, A.C., Gilson, S.-P., 2024. The chronology of the human colonization of the Canary Islands. Proc. Natl. Acad. Sci. 121, e2302924121. https://doi.org/10.1073/pnas.2302924121.

Schweingruber, F.H., 1990. Anatomy of European Woods. Paul Haupt, Bern.

Serrano, M., Pavón-Carrasco, F.J., Campuzano, S.A., Osete, M.L., 2024. ArchaeoPyDating: a new user-friendly release for archaeomagnetic dating. Archaeometry 66, 1424–1437. https://doi.org/10.1111/arcm.13009.

Siebert, L., Cottrell, E., Venzke, E., Andrews, B., 2015. Earth's volcanoes and their eruptions: an overview. Encycloped. Volcano. 239–255.

Silver, P.G., Russo Raymond, M., Lithgow-Bertelloni, Carolina, 1998. Coupling of South American and African plate motion and plate deformation. Science 279, 60–63. https://doi.org/10.1126/science.279.5347.60.

Stuiver, M., Polach, H.A., 1977. Discussion reporting of 14C data. Radiocarbon 19, 355–363. https://doi.org/10.1017/S0033822200003672.

Sveinbjörnsdóttir, Á.E., Heinemeier, J., Rud, N., Johnsen, S.J., 1992. Radiocarbon Anomalies observed for plants growing in Icelandic geothermal waters. Radiocarbon 34, 696–703. https://doi.org/10.1017/S0033822200063980.

Széréméta, N., Laj, C., Guillou, H., Kissel, C., Mazaud, A., Carracedo, J.-C., 1999. Geomagnetic paleosecular variation in the Brunhes period, from the island of El Hierro (Canary Islands). Earth Planet Sci. Lett. 165, 241–253. https://doi.org/10.1016/S0012-821X(98)00270-2.

Tilling, R.I., 1989. Volcanic hazards and their mitigation: Progress and problems. Rev. Geophys. 27, 237–269. https://doi.org/10.1029/RG027i002p00237.

UNESCO, 2023. El Hierro UNESCO global Geopark (Spain). Earth Sci. https://www.unesco.org/en/iggp/el-hierro-unesco-global-geopark accessed 12.9.24.

Urgeles, R., Canals, M., Baraza, J., Alonso, B., Masson, D., 1997. The most recent megalandslides of the Canary Islands: el Golfo debris avalanche and Canary debris flow, west El Hierro Island. J. Geophys. Res. Solid Earth 102, 20305–20323. https://doi.org/10.1029/97JB00649.

Vashakidze, G., Goguitchaichvili, A., García-Redondo, N., Calvo-Rathert, M., Carrancho, Á., Cejudo, R., Morales, J., Lebedev, V.A., Gabarashvili, K., 2019. Magnetic dating of the Holocene monogenetic Tkarsheti volcano in the Kazbeki region (great Caucasus). Earth Planets Space 71, 133. https://doi.org/10.1186/s40623-019-1109-4.

Villasante-Marcos, V., Pavón-Carrasco, F.J., 2014. Palaeomagnetic constraints on the age of Lomo Negro volcanic eruption (El Hierro, Canary Islands). Geophys. J. Int. 199, 1497–1514. https://doi.org/10.1093/gji/ggu346.

Walter, O., 1894. Petrographische studien an gesteinen der InsEl Hierro (Ph. D. Thesis). Vereinigte Friedrichs-Universität Halle-Wittenberg.

Zaczek, K., Troll, V.R., Cachao, M., Ferreira, J., Deegan, F.M., Carracedo, J.C., Soler, V., Meade, F.C., Burchardt, S., 2015. Nannofossils in 2011 El Hierro eruptive products reinstate plume model for Canary Islands. Sci. Rep. 5, 7945. https://doi.org/10.1038/srep07945.

Zazzo, A., Lepetz, S., 2017. Pompeii AD 79: a natural bone diagenesis experiment. Radiocarbon 59, 647–658. https://doi.org/10.1017/RDC.2016.28.